Microstrip Low Pass Filter Realized By EBGS Assisted T-Line

by

Mohammad Amanullah

A project submitted in partial fulfillment of the requirement for the degree of
Master of Science in Electrical and Electronic Engineering

Supervised by

Prof. Dr. Md. Nurunnabi Mollah

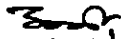Department of Electrical and Electronic Engineering

Khulna University of Engineering & Technology

Khulna -9203, Bangladesh.

June -2019

Declaration

This is to certify that the project work entitled *"MICROSTRIP LOW PASS FILTER REALIZED BY EBGS ASSISTED T- LINE"* has been carried out by **Mohammad Amanullah** in the *Department of Electrical and Electronic Engineering*, Khulna University of Engineering and Technology, Khulna, Bangladesh. The above project work or any part of this work has not been submitted anywhere for the award of any degree or diploma.
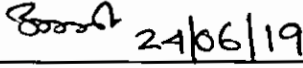
24|06|19
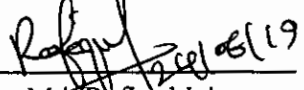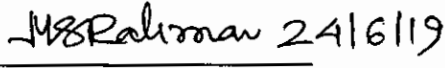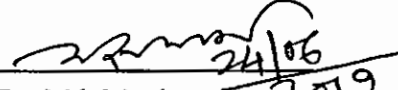Signature of the Supervisor

24-06-19
Signature of the Candidate

Approval

This project entitled "Microstrip Low Pass Filter Realized By EBGS Assisted T-Line" by Mohammad Amanullah has been approved by the board of examiners for the partial fulfillment of the requirements for the degree of Master of Science in Engineering (M. Sc. Engg.) in the Department of Electrical and Electronic Engineering, Khulna University of Engineering & Technology (KUET), Khulna, Bangladesh on June 2019.

BOARD OF EXAMINERS

1.   Chairman

   _____ 24/06/19   (Supervisor)

   Prof. Dr. Md. Nurunnabi Mollah
   Department of Electrical and Electronic Engineering
   Khulna University of Engineering & Technology
   Khulna, Bangladesh

2.   Member

   _____ 24/06/19

   Prof. Dr. Md. Rafiqul Islam
   Head of the Department
   Electrical and Electronic Engineering
   Khulna University of Engineering & Technology
   Khulna, Bangladesh

3.   Member

   _____ MSRahman 24/6/19

   Prof. Dr. Mohammad Shaifur Rahman
   Department of Electrical and Electronic Engineering
   Khulna University of Engineering & Technology
   Khulna, Bangladesh

4.   Member

   _____ 24.06.2019

   Prof. Dr. Md. Sherajul Islam
   Department of Electrical and Electronic Engineering
   Khulna University of Engineering & Technology
   Khulna, Bangladesh

5.   Member

   _____ 24/06/2019   (External)

   Prof. Dr. Md. Maniruzzaman
   Electronics and Communication Engineering Discipline
   Khulna University
   Khulna, Bangladesh

Acknowledgment

.

.   Mohammad Amanullah

Abstract

The EBGSs provide passband and stopband performance. In this project the planar conventional structures and the defected ground structures have been described. In uniform conventional structures (circular, rectangular and triangular pattern) it is observed in the scattering parameter performance that the number and the depth of the ripple (-5 db) of the passband are high and the stopband is not much wider. Maximum 10 dB RL bandwidth is 7.4 GHz, the 20 dB rejection bandwidth is 4.8 GHz and the center frequency is 10GHz. The maximum value of isolation is found to be 54dB. Then, the structures with different filling factor (FF), different number of element and same area of different structures are investigated. Then, the results of non-uniform conventional are observed and the results are ripple free in passband. The 10 dB passband RL BW is found to be 6.88 GHz and the 20 dB rejection bandwidth is not found with maximum isolation of 13.26 dB. Next the uniform dumbbell shaped DGS is observed. The 20 dB rejection bandwidth is 4 GHz. The maximum value of isolation is found to be 62 dB. The 3dB cutoff frequency is shifted to 4GHz which provides more than 200% compactness from the conventional structure. Next the result of non-uniform dumbbell shaped DGS have been observed and 10 dB RL-BW is 4.4 GHz, 3 dB cut-off frequency is 4.2 GHz, 20 dB IL-BW is 17.5 GHz and maximum peak of IL is -55 dB have been found. Finally, the hybrid dumbbell shaped DGS is observed and we have found the best performance. The best performance of 10 dB RL-BW is 4.1 GHz, 3 dB cut-off frequency is 4.4 GHz, 20 dB IL-BW is more than 19 GHz and maximum peak of IL is -68 dB. So, we have found the best performance in the hybrid dumbbell shaped DGSs. The designs are more compact than the conventional designs and able to remove the unwanted spurious transmission in the band rejection region.

Finally, the insertion loss (IL) and return loss (RL) performances of the LPFs (non-uniform triangular dumbbell shaped DGSs and hybrid DGSs) have been compared. It is seen that they provide improved performance in terms of the ripple suppression in the passband and IL bandwidths. Thus we have realized microwave LPF by EBGS assisted T-Lines.At last the physical representation of designs and the validification of the results are provided as for the validification of the work.

Contents

Chapter 1: Introduction

Chapter 2: Literature Survey

Chapter 3: Conventional LPF Design

Chapter 4: Electromagnetic Bandgap Structures

Chapter 5:Non-uniform EBGS for LPF

Chapter 6: Conclusions

List of Figures

List of Tables

List of Abbreviations

EBGS	:	Electromagnetic Bandgap Structure
PBGS	:	Photonic Bandgap Structure
UPBGS	:	Uniform PBGS
UWB	:	Ultra Wideband
SAR	:	Specific Absorption Rate
FF	:	Filling Factor
BPF	:	Bandpass Filter
DS-DGS	:	Dumbbell shaped Defected Ground Structure
DGS	:	Defected Ground Structure
MEMS	:	Micro Electro Mechanical Systems
CPW	:	Coplanar Waveguide
AMC	:	Artificial Magnetic Conducting
UC-PBG	:	Uniplanar Compact-Photonic Bandgap
EM	:	Electromagnetic
PC	:	Photonic crystal
1-D	:	One-dimensional
2-D	:	Two-dimensional
3-D	:	Three-dimensional
IL	:	Insertion Loss
RL	:	Return Loss
SWS	:	Slow wave structures
TEM	:	Transverse Electric and Magnetic
MOM	:	Method of Moments
dB	:	Decibel
BW	:	Bandwidth
LPF	:	Lowpass Filter
FSS	:	Frequency Selective Surfaces
VNA	:	Vector Network Analyzer

List of Major Symbols

ε_{eff}	:	Effective Relative Permittivity
γ	:	Propagation Constant
ω	:	Angular Frequency
β	:	Phase Constant
k	:	Wave Number (/m)
C_0	:	Speed of Light in Free Space
λ_g	:	Guided Wavelength
λ_0	:	Wavelength in Air
Z_0	:	Characteristic Impedance
f_0	:	Center Frequency
S	:	Scattering Parameters
ε_r	:	Dielectric Constant
α	:	Attenuation Constant

Chapter-1

Introduction

1.1. Introduction

A method or device that eliminates the undesirable features or shapes from a signal is called the filter. Filtering is a category of signal processing. The primary characteristic of the filters is to partial or complete restraining of the signal. This means to remove some frequencies or frequency bands. However, filters do not merely act in the frequency domain, which is in the area of image processing. Many other targets for filtering are existed. Correlations can be withdrawn for certain frequency components and not for others without having to act in the frequency domain. Filters are used in electronics and telecommunication, radio, TV, audio recordings, radar, control systems, music synthesis, computer graphics and image processing. There are several filters which overlap in several ways. Filters could be linear/ non-linear and time-invariant/ time-variant which is also called shift invariance. Filters also may be causal/not-causal, analog/digital, discrete-time/continuous-time, passive/ active type of continuous-time filter and infinite impulse response/ finite impulse response type of discrete-time filter or digital filter.

Some as usual terms used to define and classify linear filters:
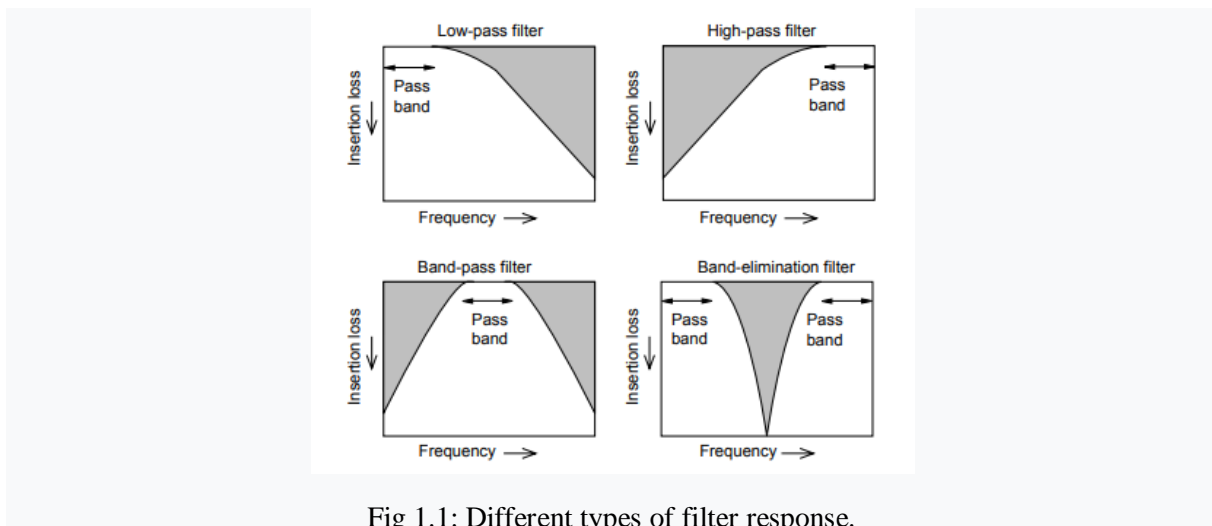
Fig 1.1: Different types of filter response.

- Low-pass filter (LPF) – Low frequencies are passed and high frequencies are attenuated.
- High-pass filter (HPF) – High frequencies are passed and low frequencies are attenuated.
- Band-pass filter (BPF) – Frequencies in a frequency band is passed.
- Band-stop filter (BSF) – Frequencies in a frequency band are attenuated.
- Notch filter (NF) – Rejects just one specific frequency.
- Comb filter (CF) – CF has multiple regularly spaced narrow pass bands giving the bandform the appearance of a comb.

- **Low Pass Filter (LPF)**

Low pass filter is a filter which passes lower frequency and attenuates high frequency signals. In communication engineering the filter of low pass, high pass and band pass provides the huge applications. LPF is the opposite of the HPF. There are different forms of LPF. They are the hiss filter used in audio, anti-aliasing filters for conditioning signals prior to analog to digital confabulation, digital filters are for acoustic barriers, data-smoothing, image-blurring etc. The moving average activities used in fields is particular kinds of LPF which can be experimented with the same signal processing techniques as are used for other LPFs. Usually, LPFs provide a low frequency signal pass with eliminations of bandpass oscillations and leave the longer-term aptitude.

Some very significant descriptions Because of the design of filters are bandwidth, frequency range, stopband attenuation, Insertion loss input and output impedance levels, group delay, VSWR, temperature range, transient response and phase linearity. The input of a filter is guided by a signal generator with the output passing to a load. At the input plane of the filter, the power may be broken into some components which are the generator incident power and the power reflected back to the generator, absorbed by the filter and passed on to the load.

1.2. Electromagnetic Bandgap Structures (EBGS)

Recently, a technology is the key to develop the wideband for microstrip antennas and filters which maneuvers the substrate is called the photonic crystals. It maneuvers the substrate in the way that surface waves are completely restrained from forming; resulting in developments in antenna efficiency and bandwidth, while minimizing side-lobes and electromagnetic interference levels. This is also known as electromagnetic bandgap structures and electromagnetic band-gap materials and the popularity is grown day by day. They are a class of periodic metallic, dielectric, or composite structures that exhibit a restrained band, or bandgap, of frequencies in which wave's incident at various directions destructively interfere and those are enable to propagate. The potential of EBGSs are not fully revealed but they have the applications of filters, antennas, waveguides, phased arrays, and many other microwave devices and components in recent days [1]. New companies and researchers have also begun to take advantages the commercial possibility of this technology [2].

EBGSs collaborate with the propagation of EM waves in a specified band of frequencies for all polarization states [3]. EBGSs are used as a microwave device. These are used to improve the gains and decrease the losses in the application of transmission. These are also known as the high impedance surface due to their capacity to put down the surface wave at certain operational frequencies. In recent days EBGS's swift growth can be look after on EM filter and antenna group [4-5].

The illustrative design of the EBG structure (square pattering 2-D structure underneath the T-line) is shown in figure below:
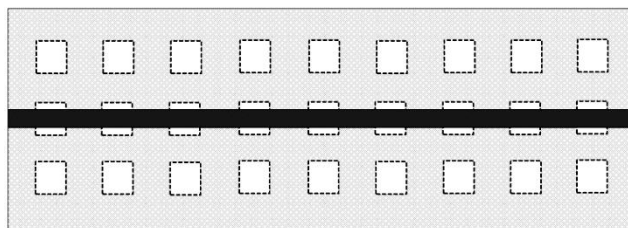
Fig 1.2: Graphical representation of 3 rows (2-D) of uniform square EBGSs beneath the T-line.

The performance of such geometry is shown below:
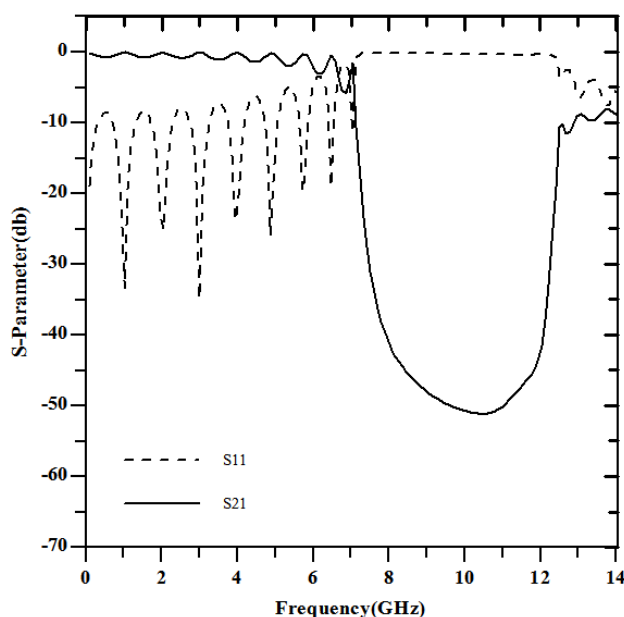
Fig 1.3: S-Parameter performances of three lines uniform square-pattering EBGSs. Here the dotted line is called the Return Loss (RL) (S11), and the solid line is called the Insertion Loss (IL) (S21)

From the above figure, it is seen that the EBGS can provide passband and stopband properties. Eli Yablonovitch and Sajeev John in 1987 breaks the traditional microwave circuit confined design to surface components and distributions of the medium circuit plane [6-7]. In the 1980s Eli Yablonovitch stated that this EBG, produced by periodic variation in the refractive index of the structure, can be very useful as it could be used to eliminate the impulsive emission of photons at certain frequency bands. Eli Yablonovitch introduced the band gap which can monitor radiation of light arbitrarily induced, and Sajeev John had submitted band gap which can reflect on light waves into focus. The idea of staking on the Bragg's condition to construct materials that block all incoming light of a particular wavelength are used by them [6].

Yablonovitch had been published about to establish periodic variation using EBG crystals as his review letter. He works on the shaping the crystal structure of millimeter drilling holes into a high dielectric constant material known as "Yablonovitch". It prohibits incident microwave signals from propagating in various directions. This explicit the 3-D Band Gap.

Researchers have mentioned the ability of materials that reflect certain EM frequencies. This valuable achievement has been spread out through the scientific community.

In 1990, Ho, Chan and Soukoulis introduced a computational demonstration of EBG band structure. From 1990, there had been several works on quantum electrodynamics in an EBG. In 1991, the 2D system of EBG had experimented by S. Shultz and 3D system of EBG had experimented by A. Z. Genack & N, Garcia. In 1995, large scale 2D EBG macroporous silicon had introduced by U. Gruning and V. Lehman and woodpile structures had been introduced by E. Ozbay, S. Noda and S. Lin. That photonic bandgap structure obtained by stacking Alumina rods and the gap is within 12 and 14 GHz [8]. In recent, some works on defected ground structures are established by Rafiquzzaman, Abu Talha Sadi and M. N. Mollah [9].

EBG applications are existing in the region of the microwave and low millimeter-wave such as electronically scanned phased arrays, high-precision GPS, Bluetooth, mobile telephony, waveguides, antennas, low loss-coplanar lines, and compactly integrated filters [10–14]. This design structures stops some operating modes and control harmonics especially for ultra-wideband (UWB) applications where other application has existence. The other exciting application of EBGSs are the reduction of absorption rate into the mobile phone operator's hand and head by its' shielding property [15–17] and protects the antennas from unwanted multipath signals which is very important in multipoint telecommunication system. In microwave engineering where using filters EBGS provides spurious passband [18]. A standard waveguide can be modified by placing of EM crystal on the two sidewalls of a waveguide. This potentially creates efficient waveguiding structure [19].

From four forms of these structures like bumpy surface, corrugated surface, metal pad or high-impedance surface and planar EBGSs we choose the planner EBGSs. The ground surface is engraved by EBGSs. EBGSs may be uniform or non-uniform and they provide different S-parameter performances for their different shapes and sizes. They are also called the photonic bandgap structures. EBG components are located beneath the T-line on the ground plane to show their ability to generate stopband performance. They also used for harmonic suppression of the filter. Slow wave property is used because of the compact design. In practical field, applications of those structures are to improve their performances in resonators, amplifiers, mixers, filters, waveguides, antennas, and many other devices.

- **Application of EBGS**

In microwave engineering, the communication system requires exclusive, reduced size, and minimal effort devices. Some new structures like Electromagnetic Bandgap Structure (EBGS), Defected Ground Structure (DGS), and Substrate integrate waveguide (SIW) and so forth are to satisfy the prerequisite and to upgrade execution are existed in this system.

As of late, numerous specialists gave more consideration to EBGSs because of their remarkable properties. Main applications of the EBGS are:

1. Resonators

2. Filters
3. Waveguides
4. Microwave devices

1.3.   The objectives of the Project

The main objective of this project is to design microstrip LPF realized by EBGSs assisted T-line. Our main goal is to gain wider, deeper and steeper LPF characteristics using the ground surface of an ideal T-line. Firstly, we need to select proper EBG unit, which will generate proper passband and stopband characteristics of the designed frequency. This project describes mainly circular, triangular, square, rectangular, triangular and triangular dumbbell shaped EBGSs. Filling factor (FF) controls the width and altitude of the stopband [20]. The concept of increasing the stopband is the enhancement of FF. This research will be carried out on non-uniform EBGSs with Binomial [21] and *Chebyshev* distributions [22]. The propagations of the EBG components are calculated as per the coefficients of the distributions. But for keeping the less ripple binomial distribution and with its hybrid structures are used in this project. In the open literature, researchers used Dumbbell-shaped DGS structures having non-uniform distributions to improve the performance of the LPF design [23]. Attention will be focused to develop LPF performance by the engraved ground surface only. Finally, triangular dumbbell-shaped DGSs will be investigated and measure their S-Parameter performances and validification of the result will be clarified. And then some fabricated designs will be shown Because of the realization and future work.

The objectives of this project are:

➢ Designing a low pass filter (LPF) over a 50 Ω T-line assisted with EBGS in the ground surface of the T-line which will provide distinct passband and stopband properties.
➢ Implementation of 1-D EBGSs (Conventional EBGS and DGS) instead of 2-D EBGSs in case of LPF design.
➢ The investigation into non-uniform Dumbbell-shaped DGSs to realize ripple free passband and wider stopband.
➢ Implementation of uniform and non-uniform EBGS and dumbbell-shaped DGS components to improve the performance of the LPF.
➢ Realization of a PBG/EBG assisted LPF structure.

1.4.   Project Outline

Project outlines are discussed below:

- In **chapter 1**, at first the introductory discussions of the project are reported. This chapter provides the primary idea about the filter and the EBGSs with its historical background. The objective of the project and outlines are also mentioned in this chapter.
- In **chapter 2**, a detailed literature survey of EBGSs is reported. The investigations of the previous researchers are reported in this chapter.
- In **chapter 3**, T-lines, microwave filters and their network analysis have been discussed in details that results in the reasoning and the proposition of modified structures comparing the available structures in the literature.
- In **chapter 4**, uniform EBGSs and dumbbell-shaped DGSs have been reported to see their performance. The 2-D and 1-D structures have been reported and described the reasoning

about choosing the 1-D structure instead of 3-D structures. Effects on different shapes and number of EBGS have been discussed. Conventional dumbbell shaped DGS has been reported and reason for choosing dumbbell shaped DGS instead of EBGS has been reported.

- In **chapter 5**, non-uniform EBGSs, triangular dumbbell-shaped DGSs and hybrid triangular DGSs have been reported to see their improved performance over conventional regular EBGSs.

- In **chapter 6**, conclusions and recommendation for future works have been presented.

Chapter-2

Literature Survey

2.1 Introduction

The implementation of EBGSs in all fields of high-frequency design is gaining extensive use. The usages for antennas include microwave filters, low-profile antennas, phased arrays, on-chip antennas and waveguides. This project is a worthy mode for this subject. Various works on the recent development of EBGSs has been expressed in this chapter. These structures are found to multiplying the performances of microwave components and devices. By restraining surface waves, leakage, and spurious transmission the stopband characteristic of EBGSs gives a significant improvement. In the literature, for uniform circular and rectangular pattering EBGSs, the optimum filling factors are considered. These types of designs are considered as the conventional EBG structure design. Besides, the researchers have worked out on dumbbell-shaped and non uniform pattering EBGS.

2.2 Applications of EBGSs

There are several applications of EBGSs. Applications of EBGSs are discussed below.

- **Resonators**

A technology of EBGSs presents resonators as an alternative to current technologies [24-27]. Structures can be made by using inexpensive standard printed circuit board (PCB) processing technique. It can be used in several commercial products. Euler and Papapolymeror already presented a literature of micro-machined resonator at 45 GHz. It is based on defect induced EBG covered with high quality factor and low losses [24].

- **Filters**

High-quality factor filters are also created by some researchers [24, 25], with high isolation [26] and low ILs with wide bandwidth [26, 27].

High isolation with a high quality factor is the main theme for EBGSs that can integrate monolithically with other components. Chappel showed 2, 3, and 6 pole filters using mettalo-dielectric EBG lattice. Also using the high-k ceramics Chappel designed a wide bandgap structure which was studded into a polymer to create a substrate for the EBGSs. Vardaxoglu reported a tunable wide bandgap using mettalo-dielectric EBGSs [28]. Hell presented a reconfigurable EBG cavity resonator with low ILs [29]. Filter application using EBGS are expressed in different ways [19, 30-33]. Radistic researched on circular three line structures in the ground surface of the circuit of microwave devices [30].

- **LPF using Uniplanar Compact (UC) EBGSs**

UC-EBGSs are made by using the 2-D compact structures with the slow wave effect. Fei-Ran Yang presented a coupled microstrip LPF with a spurious-free bandpass filter and high-performance [30]. These structures used to improve the performance of conventional LPF on the ground surface [30]. Between the structures a small 50 Ω feed line is established on the ground surface. Here they used the droid substrate with ε_r = 10.2, thickness = 25 mils and width of the 50 Ω microstrip T-line is 24 mils. The result of the simulation performed wider stopband of near about 6 GHz and S_{21} is achieved below -30 dB for a wide range of frequency. For this structure stepped-impedance LPF with 7 (seven) reactive components have been chosen with indicating poor radiation loss which verifies also the EBG property [34].
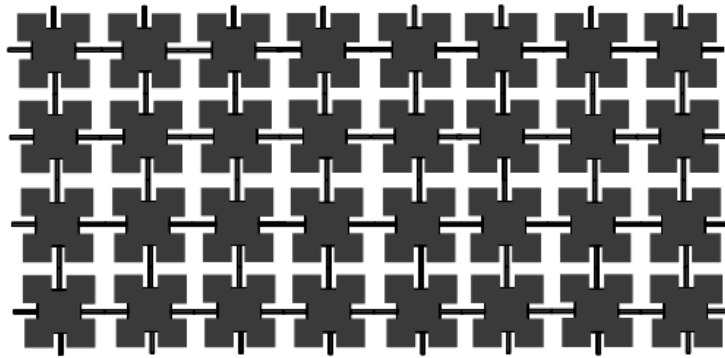
Fig 2.1: Structure of UC-EBG

- **Bandpass Filters (BPFs)**

Band pass filter is parallel coupled. EBGs can avoid using of extra filters to achieve a compact microstrip BPF which rejects unwanted signals [35]. Here researchers used a UC-EBG on the ground surface as a low loss T-line. Here unwanted harmonics can be restrained with the help of EBGS and performed wider and deeper stopband. Figure describes the conventional microstrip BPF on the UC-EBG on the ground plane.
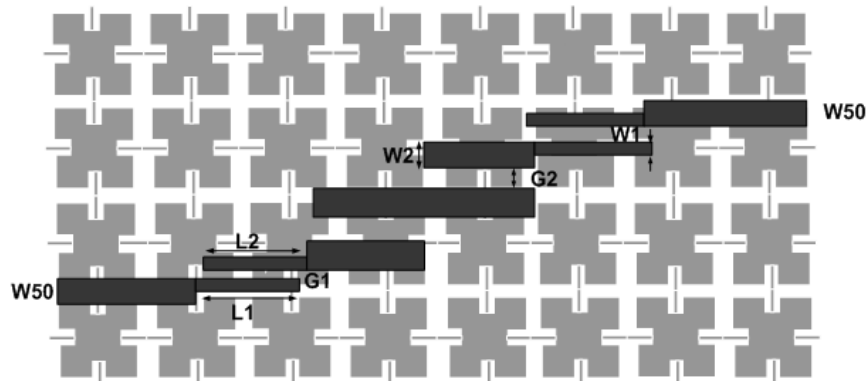
Fig 2.2: Conventional diagram of a BPF over UC-EBGs

From the reference papers we have got the design procedures of the parallel coupled Band pass filters [35]. Researchers had used the frequency of 12 and 17 GHz and transmission coefficient used as -10 and -5 dB. This filter provides the spurious restraining of 30dB to 40dB. Due to the slow wave factor and same coupling gap they got the increased fractional bandwidth at 6 GHz center frequency. This UC-EBG assisted BPF also improved the BPF performance by the optimum coupling co-efficiency. The least IL of this filter is get to be 1.9dB at 6.39GHz including the connector of the circuit.

Loptegi had also schemed different BPF using DGSs [19]. Nesic presented an EBG microstrip slow wave structure which achieved slow wave and LPF characteristics. But a modified microstrip line was used for its fabrication, without engraving the ground surface [31-33].

2.3   Microwave Devices using EBGS

Micro-machined capacitive bridge used to achieve a EBG assisted tunable filter for its design, simulation and fabrication [36]. MEMS switches based on EBG co-planar waveguides were planned and tuned for wider bandstop filter [37]. These structures are based on ferroelectric or ferromagnetic thin films are also found in previous research papers [38]. Ferroelectric capacitors are also considered for tuning the performance of EBGSs [36, 39]. Ferroelectric varactors are deliberated to achieve tunable EBG performance in L-C circuits for periodically loading CPWs. Asymmetric or symmetric tuning of the bandgap width was attained by altering the capacitance of the varactors in L-C circuits [38]. Yongje had given a unique idea to get the EBGS with a wide tunable stopband filter mistreatment DS-DGS [40]. Miguel had raised a multiple frequencies tuned PBGS [41].

2.4   Compactness of EBG structured devices

In recent compactness of devices are too much essential. EBGSs are found to compact the device structures. A magnetic conductor is presented by Roger for its reduced size and cost [42]. For the reduction of the number of EBG cells, the capacitance and the inductance need to be raised [43]. Feresidis was first presented the concept of closely coupled metallo dielectric EBGSs and worked on 2-D double layer closely packed dipole arrays [44]. Small, lightweight and compactness are the main requirement in modern wireless communication system. At outside the band gap frequencies, periodic structures accept slow waves, with lessen phase velocity and guided wavelength with respect to the wave propagating in an analogous homogeneous medium. The miniaturization of microwave components like the triple array components exploited this property [45] and to examine the components with periodic loading. Multiple-order periodic loading of basic components occupies a good degree of flexibility in the design [45, 46]. In recent, uniform EBG with offset T-line and dumbbell shaped EBGS with periodic structure has been proposed by S. M. Shakil Hassan and M. N. Mollah. From those literatures we can learn the idea of compactness of the microwave devices.

Fig 2.3: Offset in uniform EBGS assisted T-line [47]
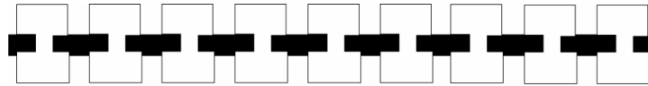
Fig 2.4: EBGS assisted microstrip T-line having Dumbbell shaped EBGS with rectangular bigger slots [48]

Fractal-type structures are eventually produced. They are used for multiband artificial magnetic conducting designs [46]. There is another way of increasing the loading stubs length without increasing the cell of the unit and capacitive coupling within successive components. This is called the inter-digital technology. The loadings of consecutive dipoles are shifted. They can be extended to the full length approved by the array geometry.

2.5   Uniform and Non-Uniform Structures

Conventional EBG structures are usually uniform. But there are also non-uniform EBGSs we can find in the previous literature [9]. Researchers have developed EBGS of different sizes and shapes [47-48]. Also hybrid structures have developed in recent days. Uniform conventional structures give low stopband width and rippled passband performance. This recovers non-uniform structures. Binomial, *Chebychev*, Gaussian etc structures are used for finding the amplitude of the structures. This results much satisfactory performance. In recent hybrid structures are more popular. Conventional EBGSs are placed between the defected ground structures and those inter-element spaced element could be uniform or non uniform. Researchers found those hybrid structures performances as more interesting with respect to the ripple free passband and wider stopband with deeper insertion loss performance.

Chapter-3
Conventional LPF Design

3.1. Introduction:

Due to the nature of the structures, periodic structures are generally showed the passband and stopband characteristics. In case of waves in crystalline lattice structures this was initially studied. The results are more common. By inspection of the k-β or ω-β diagram the presence or absence of propagating wave can be destined. For our project work it is necessary the rise and down the passband or stopband structures. We should study the characteristics and parameters of the structures. We also need to study the LPF prototypes. Theoretically we will show the lumped element conventional structures and several graphical presentation will be noticed for the lumped element filter. The main objectives of this chapter are to recite two-port network concepts, network parameters, and periodic structures and provide equations that are useful because of the analysis of filter networks.

3.2. Scattering Parameters or S-Parameters:

The S parameters of a two-port network could be shown as:

$$S_{11} = \frac{b_1}{a_1}\bigg|_{a_2=0} \quad S_{12} = \frac{b_1}{a_2}\bigg|_{a_1=0} \tag{3.1}$$

$$S_{21} = \frac{b_2}{a_1}\bigg|_{a_2=0} \quad S_{22} = \frac{b_2}{a_2}\bigg|_{a_1=0}$$

Where $a_n = 0$ describes a perfect impedance match at port n. These resolutions may be written as

$$\begin{bmatrix} b_1 \\ b_2 \end{bmatrix} = \begin{bmatrix} S_{11} & S_{12} \\ S_{21} & S_{22} \end{bmatrix} \begin{bmatrix} a_1 \\ a_2 \end{bmatrix} \tag{3.2}$$

Scattering matrix may be simply denoted by [S].

The parameters S_{11} and S_{22} are also known as the reflection coefficients, whereas S_{12} and S_{21} the transmission coefficients. These are the parameters immediately quantifiable at microwave frequencies. The S parameters are usually complex, and it is advantageous to express them in terms of propagations and phases, i.e., $S_{mn} = |S_{mn}|e^{j\phi_{mn}}$ for m, n = 1, 2. Often their propagations are given in decibels (dB), which are defined as

$$20\log|S_{mn}| \ dB \quad m,n = 1,2 \tag{3.3}$$

Where the logarithm operation is base 10. For filter characterization, we may explain two parameters:

$$L_A = -20\log|S_{mn}| \ dB \quad m,n = 1,2 \ (m \neq n) \tag{3.4}$$

$$L_R = -20 \log|S_{nn}| \; dB \quad n = 1,2$$

Where L_A denotes the IL within ports n and m and L_R illustrates the RL at port n. In lieu of applying the RL, the voltage standing wave ratio (VSWR) may be used. The definition of VSWR is expressed by this equation

$$VSWR = \frac{1 + |S_{nn}|}{1 - |S_{nn}|} \tag{3.5}$$

Fig 3.1.   Symmetrical two-port network

$$\text{RL}, S_{11} = 20 \; log_{10}\left(\frac{V_r}{V_i}\right)$$

$$= 10 \; log_{10}\left(\frac{p_r}{p_i}\right) \tag{3.6}$$

$$\text{IL}, S_{21} = 20 \; log_{10}\left(\frac{V_t}{V_i}\right)$$

$$= 10 \; log_{10}\left(\frac{p_t}{p_i}\right) \tag{3.7}$$

3.3.   ABCD Parameters:

The ABCD parameters of a two-port network are expressed by

$$A = \left.\frac{V_1}{V_2}\right|_{I_2=0} \qquad B = \left.\frac{V_1}{-I_2}\right|_{V_2=0} \tag{3.8}$$

$$C = \left.\frac{I_1}{V_2}\right|_{I_2=0} \qquad D = \left.\frac{I_1}{-I_2}\right|_{V_2=0}$$

These parameters are actually defined in a set of linear equations in matrix notation

$$\begin{bmatrix} V_1 \\ I_1 \end{bmatrix} = \begin{bmatrix} A & B \\ C & D \end{bmatrix} \begin{bmatrix} V_2 \\ -I_2 \end{bmatrix} \tag{3.9}$$

Where the matrix comprised of the ABCD parameters is known as the ABCD matrix. Sometimes, it may also be referred to as the transfer or chain matrix. The ABCD parameters have the following properties:

$$\text{AD} - \text{BC} = 1 \qquad \text{For a reciprocal network} \tag{3.10}$$

$$\text{A} = \text{D} \qquad \text{For a symmetrical network} \tag{3.11}$$

If the network is lossless, then A and D will be purely real and B and C will be purely imaginary.

3.4. Microwave:

The frequency range of EM waves is 2 to 40GHz. This frequency range is known as microwave. This wave of radio handles in 2.4GHz and 5.7GHz frequency are unlicensed bands and 6-11, 13, 15, 18, 23 and 38GHz frequency are licensed band. In this range, highly directional beams are feasible and microwave is quite competent for point-to-point transmission. Higher signal to noise (SN) ratio is provided by using a parabolic antenna for achieving a small beam from all the energy. For this technology the antennas of transmission and reception should be accurately aligned to each other. This wave is a main factor in the satellite communication system.
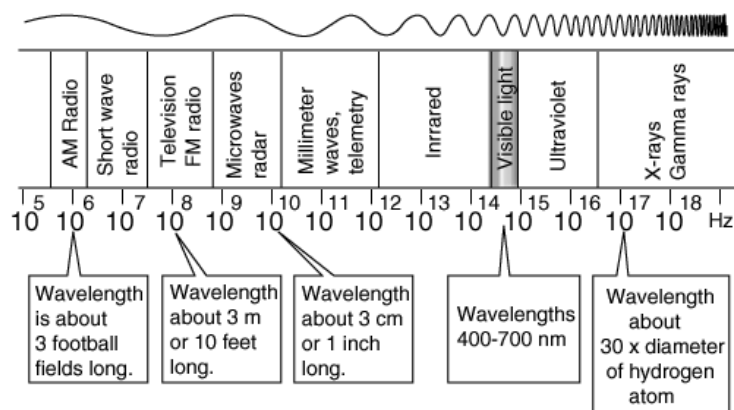
Fig 3.2. Communication Frequency spectrum

A microwave comprises a feed cables, waveguides, radios, multiplexes, and, antennas. Based on capacity and radio equipment, antenna size, tower heights and terrain evaluation will play a major role in how it will be planned and constructed the system. Some factors like capacity and radio equipment, antenna size, tower heights and terrain will play a significant role and also will dedicate system reliability, multi-path fading, fade margins calculations, freshnel zone clearance, interference analysis, system diversity and long distance specifications.

3.5. Microwave Filter:

In microwave engineering filter is the important component which main job is to eliminate unwanted signals and to receive necessary signals. A microwave filter is simply a two port network is works for controlling the frequency response among the passband or stopband. A great advantage is there are no lumped element uses in microwave system but EBG elements are used as the lumped elements there. The important thing is this filter minimizes the losses of the passband. This type of filter reduces the total loss as well as reduces the noise when it is used as a receiver.

3.6. Definition of terms used for microwave filter design:

Now we discuss below various terms which are commonly used in microwave filter:

- **Insertion Loss (IL):**

IL is identical to the variety in decibel power measured at the filter input and output. The power weighed at the filter input and the measured power is equivalent when the filter is replaced by a 100% matched network analyzer. The input impedance of the advancing instrument and the characteristic impedance should be equal. IL contains three loss factors like the impedance mismatch at the filter input or output or the dissipative loss cooperated with each reactive element within the filter.

Mathematically, IL means 10 times of the logarithmic values of the ratio of transmitting power to the incident power.

$$IL = 10 \, log_{10} \left(\frac{p_t}{p_i} \right) \tag{3.12}$$

For example,
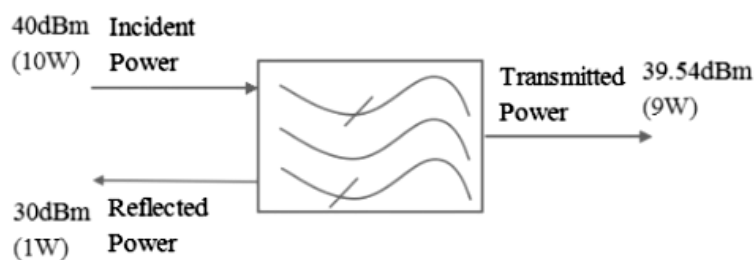
- **Return Loss (RL):**

RL defines the power-loss in the signal put back by a discontinuity in a T-line. This discontinuity can be a mismatch with the terminating load implanted in the line and is generally revealed as a ratio in decibels. RL is involved to both SWR and reflection coefficient (Γ). Increasing RL befits to poor SWR. This loss measures the wellness of devices or matched lines. If the loss is high the match is good. High RL is considerable and results in a lower IL.

Mathematically, RL means 10 times of the logarithmic values of the ratio of reflecting power and the incident power.

$$RL = 10 \, log_{10} \left(\frac{p_r}{p_i} \right) \tag{3.13}$$

For example,
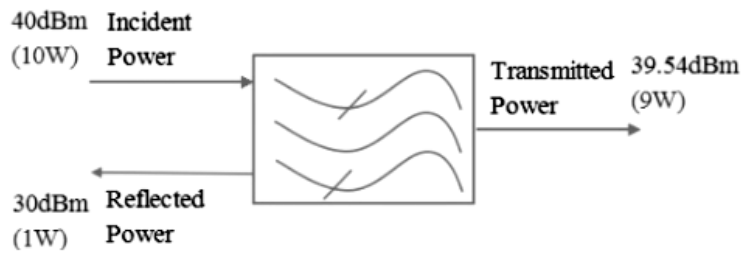
$$\text{Return Loss} = -\frac{10*Log(1W/1mW)}{10*Log(10W/1mW)} = -\frac{30dBm}{40dBm} = 10dB$$

- **Slow Wave:**

EM waves having the velocity lower than the velocity of light in free space are known as slow waves. Periodic perturbation in the ground surface provides periodic discontinuity is provided by Periodic perturbation in the ground surface. Slow wave structures have the good features for compact designs of microwave circuits.

- **Passband and ripple height:**

Passband slope should be sharper and aimed frequency should be obtained. Ripple height should be as low as possible.

- **Cut-off Frequency:**

Cut-off frequency, f_{co} is the frequency at which the filter IL is equal to 3dB. It is a very convenient point of expressing the passband and stopband boundary points. In addition, it allows a convenient means to normalize the frequency response of a filter. For example, if the frequency of a low-pass filter (LPF) response were divided by f_{co} then the resulting response would be "normalized" to f_{co}. The normalized response allows the design engineer to quickly specify the filter needed to meet his system requirements.

3.7. Periodic Structures:

An infinite T-line or waveguide periodically loaded with reactive components is an example of a periodic structure. As shown in Fig 3.5, periodic structures can take various forms, depending on the T-line media being used. Often the loading components are formed as discontinuities in the line itself, but in any case, they can be modeled as lumped reactance in shunt (or series) on a T-line, as shown in Fig 3.6. Periodic structures support slow-wave propagation (slower than the phase velocity of the unloaded line), and have passband and stopband characteristics similar to those of filters; they find application in traveling-wave tubes, masers, phase shifters, and antennas.

(a)

(b)
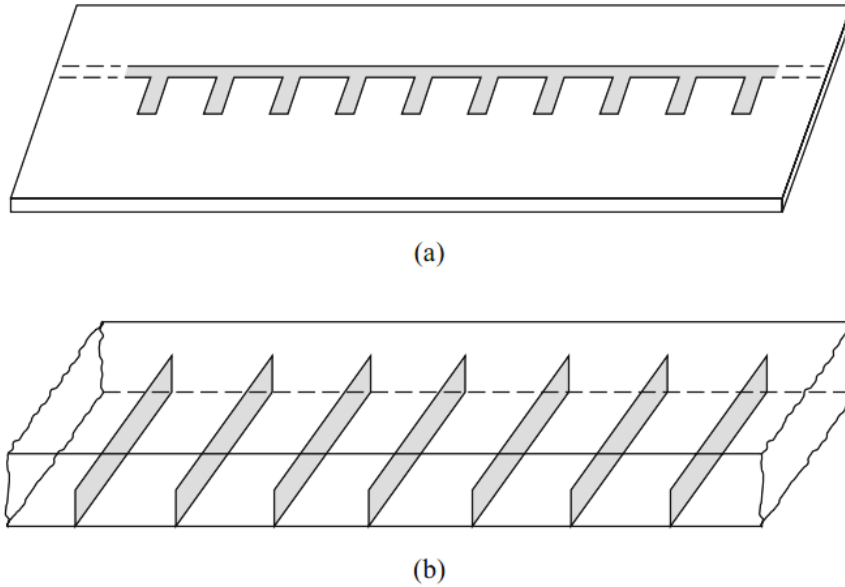
Fig 3.3. Examples of periodic structures. (a) Periodic stubs on a microstrip line. (b) Periodic diaphragms in a waveguide.
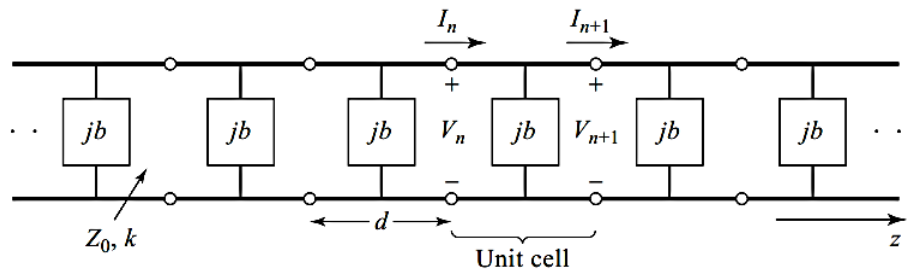
Fig 3.4. The equivalent circuit of a periodically loaded T-line. The unloaded line has characteristic impedance Z_0 and propagation constant k.

3.8. Capacitively loaded transmission-line-circuit analysis:

A simple capacitively loaded T-line can be analyzed to conceive the idea of periodic structures. The velocity of EM wave in a physically smooth T-line can be written as

$$V_p = \frac{1}{\sqrt{LC}} = \frac{1}{\sqrt{\mu_0 \varepsilon_0 \varepsilon_r}} \tag{3.14}$$

Where,

V_P is the phase velocity of the EM wave.

L is the series inductance per unit length.

C is the shunt capacitance per unit length.

ε_r is the dielectric constant of the medium surrounding the conductor.

ε_0 and μ_0 are free-space values of the permittivity and permeability respectively.

From equation (3.19) it is seen that with the value of the dielectric constant (ε_r), the phase velocity of EM waves reduces. One problem arises in this simplest way of reducing the phase velocity. If the value of the dielectric constant is increased then the higher-order mode of wave propagates. To avoid this propagation, the cross-sectional dimensions of the line must be reduced accordingly. This is the limitation of increasing the value of the dielectric constant to get the reduced value of the phase velocity of EM waves.

We know $LC = \mu_0\varepsilon$ for dielectric media. So any attempt of increasing the value of C to reduce the phase velocity is restricted here. Because if the value of C has increased the value of L will be automatically reduced to maintain the relation, $LC = \mu_0\varepsilon$ in a physically smooth T-line. Under this circumstance, the restriction of a physically smooth T-line can be relaxed instead of an electrical smooth line. An effective increase in the shunt capacitance per unit length (C) can be achieved without disturbing the value of inductance per unit length (L) by loading lumped shunt capacitance at periodic intervals where the spacing within the loaded shunt capacitance are small compared with the wavelength. At this stage, though the line is not physically smooth, it will be an electrically smooth line. Under this condition, the capacitance will be increased which can be observed from the following equation of the phase velocity.

$$V_p = \frac{1}{\sqrt{(C + C_0/d)L}} = \frac{\omega}{\beta} \tag{3.15}$$

Where C_0/d is the loaded lumped capacitance per unit length and C_0 is the capacitance loaded per interval d.

There are many ways of obtaining periodic structures. One of the simplest ways is to load a thin diaphragm at regular intervals in a coaxial T-line. The diaphragm may be machined as an integral part of the center conductor. The fringing electric field in the vicinity of the diaphragm increases the local storage of the electric energy and hence giving more extra shunt capacitance.

3.9.   Circuit Analysis of a Periodic Structure

A T-line can be considered as the combination of finite unit cells of the structure. Fig 3.5(a) is the equivalent circuit of a basic unit cell of a capacitively loaded coaxial line and Fig 3.5(b) is the complete T-line composed of the basic unit cell. The unit cell may be divided into three parts as a T-line of length d/2 on either side of normalized susceptance B.
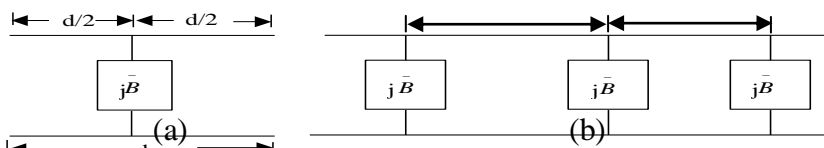
Fig 3.5. Equivalent circuit model of a unit cell, (b) a T-line cascaded by unit cells.

3.10. Analysis of Infinite Periodic Structures:

Firstly, we need to consider the propagation characteristics of the infinite loaded line shown in the previous Fig. Each unit cell of this line consists of a length, d, of the T-line with a shunt susceptance across the midpoint of the line; the susceptance, b, is normalized to the characteristic impedance, Z_0. If we consider the infinite line as being composed of a cascade of identical two-port networks, we can relate the voltages and currents on either side of the nth unit cell using the ABCD matrix:

$$\begin{bmatrix} V_n \\ I_n \end{bmatrix} = \begin{bmatrix} A & B \\ C & D \end{bmatrix} \begin{bmatrix} V_{n+1} \\ I_{n+1} \end{bmatrix} \tag{3.16}$$

Where A, B, C, and D are the matrix parameters for a cascade of a T-line section of length d/2, a shunt susceptance b, and another T-line section of length d/2. The reader can verify that $AD - BC = 1$, as required for reciprocal networks.

For a wave propagating in the + z direction, we must have

$$V(z) = V(0)e^{-\gamma z} \tag{3.17}$$

$$I(z) = I(0)e^{-\gamma z}$$

for a phase reference at z = 0. Since the structure is infinitely long, the voltage and current at the nth terminals can differ from the voltage and current at the n + 1 terminals only by the propagation factor, $e^{-\gamma d}$. Thus,

$$V_{n+1} = V_n e^{-\gamma d} \tag{3.18}$$

$$I_{n+1} = I_n e^{-\gamma d}$$

Using this result in (3.23) gives the following:

$$\begin{bmatrix} V_n \\ I_n \end{bmatrix} = \begin{bmatrix} A & B \\ C & D \end{bmatrix} \begin{bmatrix} V_{n+1} \\ I_{n+1} \end{bmatrix} = \begin{bmatrix} V_{n+1}e^{\gamma d} \\ I_{n+1}e^{\gamma d} \end{bmatrix} \tag{3.19}$$

For a nontrivial solution, the determinant of the above matrix must vanish:

$$AD + e^{2\gamma d} - (A + D)e^{\gamma d} - BC = 0 \tag{3.20}$$

or, since $AD - BC = 1$,

$$1 + e^{2\gamma d} - (A + D)e^{\gamma d} = 0$$

$$e^{-\gamma d} + e^{\gamma d} = A + D$$

$$\cosh \gamma d = \frac{A+D}{2} = \cos \theta - \frac{b}{2}\sin \theta \tag{3.21}$$

Now, if $\gamma = \alpha + j\beta$, we have that

$$\cosh \gamma d = \cosh \alpha d \cosh \beta d + j \cosh \alpha d \cosh \beta d = \cos \theta - \frac{b}{2}\sin \theta \tag{3.22}$$

Since the right-hand side of (3.36) is purely real, we must have either $\alpha = 0$ or $\beta = 0$.

In the first case, $\alpha=0$, $\beta\neq0$, which directs to a non reduced propagating wave on the periodic structure. So, we get the passband of the structure. We get from the equation,

$$\cosh \beta d = \cos \theta - \frac{b}{2} \sin \theta \qquad (3.23)$$

Which can be solved for β if the magnitude of the right-hand side is less than or equal to unity. Note that there are an infinite number of values of β that can satisfy the previous equation.

In the second case, $\alpha\neq0$, $\beta=0$, π. Which directs the wave does not propagate, but is attenuated along the line; this defines the stopband of the structure. Because the line is lossless, power is not dissipated, but is reflected back to the input of the line. The magnitude of (3.22) reduces to

$$\cosh \alpha d = \left| \cos \theta - \frac{b}{2} \sin \theta \right| \geq 1 \qquad (3.24)$$

which has only one solution $(\alpha > 0)$ for positively traveling waves; $\alpha < 0$ applies for negatively traveling waves. If $\cos\theta - (b/2)\sin \theta \leq -1$, (3.24) is obtained from (3.22) by letting $\beta = \pi$; then all the lumped loads on the line are $\lambda/2$ apart, yielding an input impedance the same as if $\beta = 0$.

3.11. Conventional LPF Design using Image Parameter Method

The image parameter method of filter design involves the specification of passband and stopband characteristics for a cascade of simple two-port networks. The method is relatively simple but has the disadvantage that an arbitrary frequency response cannot be incorporated into the design. The image parameter method also finds application in solid-state traveling-wave amplifier design. The method is explained in details below.

First imagine the image impedances and voltage transfer function for an arbitrary reciprocal two-port network; these results are required Because of the analysis and design of filters by the image parameter method. Consider the arbitrary two-port network shown in Fig. The image impedances, Z_{i1} and Z_{i2}, are defined for this network as follows:

Z_{i1}=input impedance at port 1 when port 2 is terminated with Z_{i2}

Z_{i2}=input impedance at port 2 when port 1 is terminated with Z_{i1}.

Thus both ports are matched when terminated in their image impedances. We can derive expressions Because of the image impedances in terms of the ABCD parameters of the network.
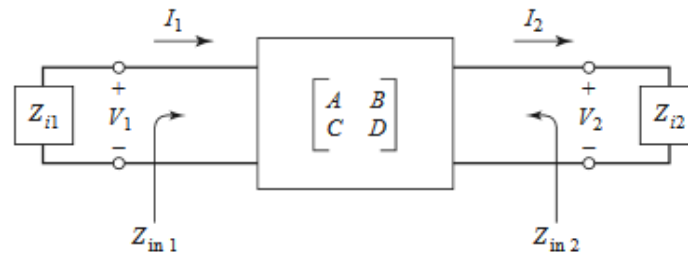
Fig 3.6. A two-port network terminated in its image impedances

The port voltages and currents are related as

$$V_1 = AV_2 + BI_2$$
$$I_1 = CV_2 + DI_2$$

The input impedance at port 1, with port 2 terminated in Z_{i2}, is

$$Z_{in1} = \frac{V_1}{I_1} = \frac{AV_2 + BI_2}{CV_2 + DI_2} = \frac{AZ_{i2} + B}{CZ_{i2} + D}$$

Since, $V_2 = Z_{i2}I_2$

Now solve above equations for V_2, I_2 by inverting the ABCD matrix. Since, AD−BC=1 for a reciprocal network, we obtain

$$V_2 = DV_1 - BI_1$$
$$I_2 = -CV_1 + AI_1$$

Then the input impedance at port 2, with port 1 terminated in Z_{i1}, can be found as

$$Z_{in2} = \frac{-V_2}{I_2} = \frac{DV_1 - BI_1}{-CV_1 + AI_1} = \frac{DZ_{i1} + B}{CZ_{i1} + A}$$

Solving for Z_{i1} and Z_{i2} gives

$$Z_{i1} = \sqrt{\frac{AB}{CD}}$$

$$Z_{i2} = \sqrt{\frac{BD}{AC}}$$

If the network is symmetric, then A=D and $Z_{i1}=Z_{i2}$ as expected.
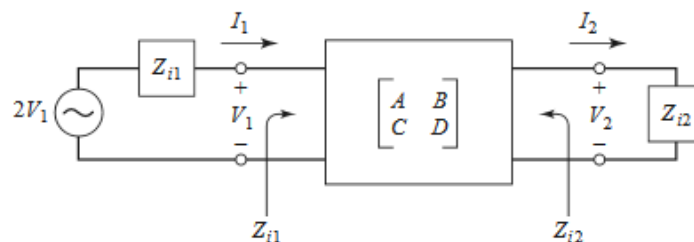
Fig 3.7. A two-port network terminated in its image impedances and driven with a voltage generator.

3.12. Conventional LPF Design using IL Method

A perfect filter would have zero IL in the passband, infinite attenuation in the stopband, and linear phase response (to avoid signal distortion) in the passband. Of course, such filters do

not exist in practice, so compromises must be made; herein lies the art of filter design. The image parameter method of the previous section may yield a usable filter response for some applications, but there is no methodical way of improving the design. The IL method, however, allows a high degree of control over the passband and stopband propagation and phase characteristics, with a systematic way to synthesize the aimed response. The necessary design trade-offs can be evaluated to best meet the application requirements. If, for example, a minimum IL is most important, a binomial response could be used; a Chebyshev response would satisfy a requirement Because of the sharpest cut-off. If it is possible to sacrifice the attenuation rate, a better phase response can be obtained by using a linear phase filter design. In addition, in all cases, the IL method allows filter performance to be improved in a straightforward manner, at the expense of a higher order filter. Because of the filter prototypes to be discussed below, the order of the filter is equal to the number of reactive components.

The steps of establishing the LPF using the IL method have been describing below. First, the Fig is shown here how to process step by step:
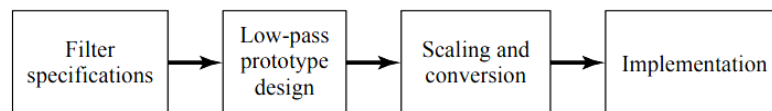
Fig 3.8. The process of filter design by the IL method.

- **Maximally Flat LPF Prototype**

The process of making LPF can be extended to find the element values for filters with an arbitrary number of components, N, but clearly this is not practical for large N. For a normalized low-pass design, where the source impedance is 1 and the cut-off frequency is ω_c = 1 rad/sec, however, the element values Because of the ladder-type circuits can be tabulated. Table 3.1 gives such element values for maximally flat LPF prototypes for N = 1 to 10. These data can be used with either of the ladder circuits in the following way. The element values are numbered from g_0 at the generator impedance to g_{N+1} at the load impedance for a filter having N reactive components.
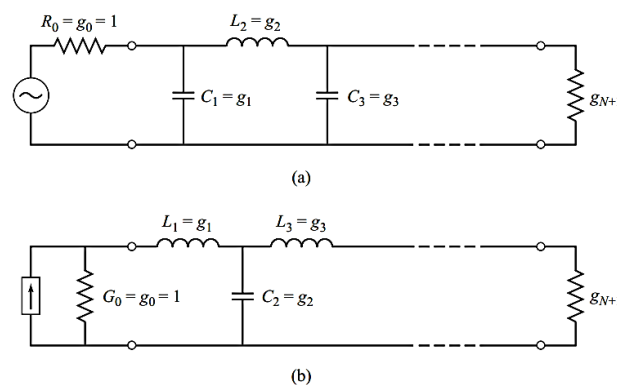
Fig 3.9. Ladder circuits for LPF prototypes and their element definitions. (a) Prototype beginning with a shunt element. (b) Prototype beginning with a series element.

The components alternate within series and shunt connections and g_k has the following definition:

g_0 = generator resistance (Fig 3.9a), generator conductance (Fig 3.9b)

g_k (k=1 to N) = inductance for series inductors, the capacitance for shunt capacitors

g_{N+1} = load resistance if g_N is a shunt capacitor, load conductance if g_N is a series inductor

Finally, as a matter of practical design procedure, it will be necessary to determine the size, or order, of the filter. This is usually dictated by a specification on the IL at some frequency in the stopband of the filter. Fig 3.10 shows the attenuation characteristics for various N versus normalized frequency. If a filter with N>10 is required, a good result can usually be obtained by cascading two designs of a lower order.
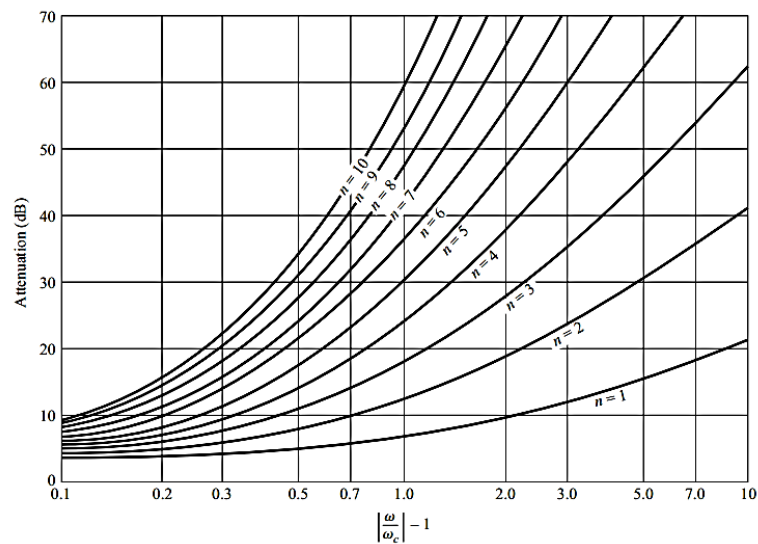
Fig 3.10. Attenuation versus normalized frequency for maximally flat filter prototypes.

Table 3.1: Element values for maximally flat, LPF prototypes (g_0=1, ω_c =1, N=1 to 10)

N	g_1	g_2	g_3	g_4	g_5	g_6	g_7	g_8	g_9	g_{10}	g_{11}
1	2.0000	1.0000									
2	1.4142	1.4142	1.0000								
3	1.0000	2.0000	1.0000	1.0000							
4	0.7654	1.8478	1.8478	0.7654	1.0000						
5	0.6180	1.6180	2.0000	1.6180	0.6180	1.0000					
6	0.5176	1.4142	1.9318	1.9318	1.4142	0.5176	1.0000				
7	0.4450	1.2470	1.8019	2.0000	1.8019	1.2470	0.4450	1.0000			
8	0.3902	1.1111	1.6629	1.9615	1.9615	1.6629	1.1111	0.3902	1.0000		
9	0.3473	1.0000	1.5321	1.8794	2.0000	1.8794	1.5321	1.0000	0.3473	1.0000	
10	0.3129	0.9080	1.4142	1.7820	1.9754	1.9754	1.7820	1.4142	0.9080	0.3129	1.0000

- **Equal-Ripple LPF Prototype**

Tables exist for designing equal-ripple LPFs with a normalized source impedance and cut-off frequency ($\omega_c = 1$rad/sec), and these can be wielded to either of the ladder circuits. This design data depends on the specified passband ripple level; Table 3.2 lists element values for normalized LPF prototypes having 0.5 or 3.0 dB ripple for N = 1 to 10. Notice that the load impedance $g_{N+1} \neq 1$ for even N . If the stopband attenuation is specified, the curves in Fig 3.10 can be used to determine the necessary value of N Because of these ripple values.
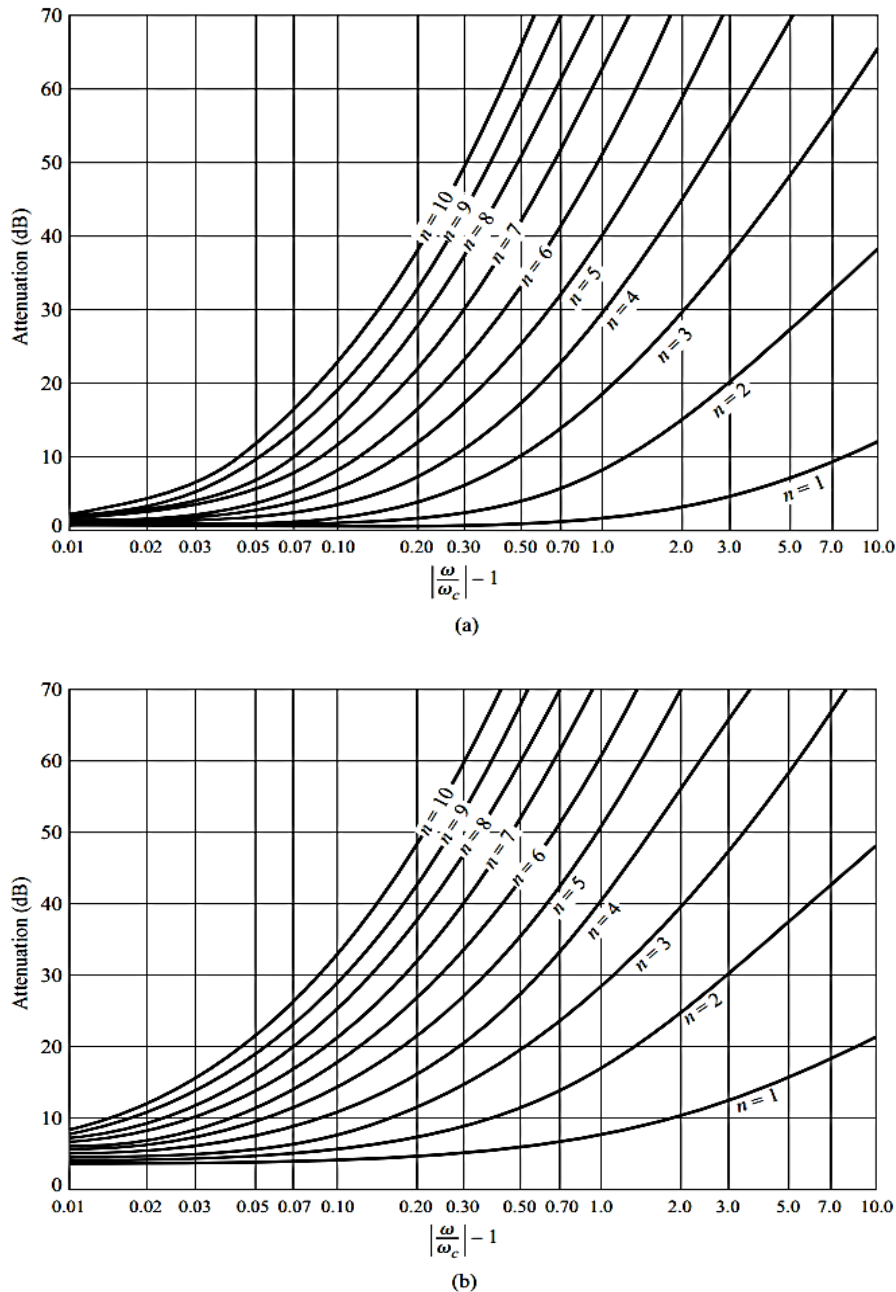
Fig 3.11.   Attenuation versus normalized frequency for equal-ripple filter prototypes. (a) 0.5 dB ripple level. (b) 3.0 dB ripple level.

Table 3.2: Element Values for Equal-Ripple LPF Prototypes (g_0= 1, ω_c =1, N = 1 to 10, 0.5 dB and 3.0 dB ripple)

N	g_1	g_2	g_3	g_4	g_5	g_6	g_7	g_8	g_9	g_{10}	g_{11}
					0.5 dB Ripple						
1	0.6986	1.0000									
2	1.4029	0.7071	1.9841								
3	1.5963	1.0967	1.5963	1.0000							
4	1.6703	1.1926	2.3661	0.8419	1.9841						
5	1.7058	1.2296	2.5408	1.2296	1.7058	1.0000					
6	1.7254	1.2479	2.6064	1.3137	2.4758	0.8696	1.9841				
7	1.7372	1.2583	2.6381	1.3444	2.6381	1.2583	1.7372	1.0000			
8	1.7451	1.2647	2.6564	1.3590	2.6964	1.3389	2.5093	0.8796	1.9841		
9	1.7504	1.2690	2.6678	1.3673	2.7239	1.3673	2.6678	1.2690	1.7504	1.0000	
10	1.7543	1.2721	2.6754	1.3725	2.7392	1.3806	2.7231	1.3485	2.5239	0.8842	1.9841
					3.0 dB Ripple						
1	1.9953	1.0000									
2	3.1013	0.5339	5.8095								
3	3.3487	0.7117	3.3487	1.0000							
4	3.4389	0.7483	4.3471	0.5920	5.8095						
5	3.4817	0.7618	4.5381	0.7618	3.4817	1.0000					
6	3.5045	0.7685	4.6061	0.7929	4.4641	0.6033	5.8095				
7	3.5182	0.7723	4.6386	0.8039	4.6386	0.7723	3.5182	1.0000			
8	3.5277	0.7745	4.6575	0.8089	4.6990	0.8018	4.4990	0.6073	5.8095		
9	3.5340	0.7760	4.6692	0.8118	4.7272	0.8118	4.6692	0.7760	3.5340	1.0000	
10	3.5384	0.7771	4.6768	0.8136	4.7425	0.8164	4.7260	0.8051	4.5142	0.6091	5.8095

- **Finalize the LPF design:**

To design a LPF for fabrication using microstrip lines. Let, the following steps are considered. The specifications include a cut-off frequency of 4 GHz, an impedance of 50 Ω, and a third-order 3 dB equal-ripple passband response. Firstly, the normalized low-pass prototype element values are taken from Table 3.2. They are:

$$g_1 = 3.3487 = L_1$$
$$g_2 = 0.7117 = C_2$$
$$g_3 = 3.3487 = L_3$$
$$g_4 = 1.0000 = R_L$$

with the lumped-element circuit shown in Fig below.

(a)
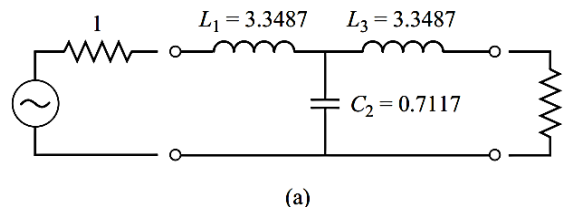
Fig 3.12. Filter design procedure. Lumped-element LPF prototype.

Now, here use Richards' transformations to convert series inductors to series stubs, and shunt capacitors to shunt stubs, as shown in Fig below. The characteristic impedance of a series stub (inductor) is L, and the characteristic impedance of a shunt stub (capacitor) is 1/C. For

commensurate line synthesis, all stubs are $\lambda/8$ long at $\omega = \omega_c$. (It is usually most convenient to work with normalized quantities until the last step in the design.)

(b)
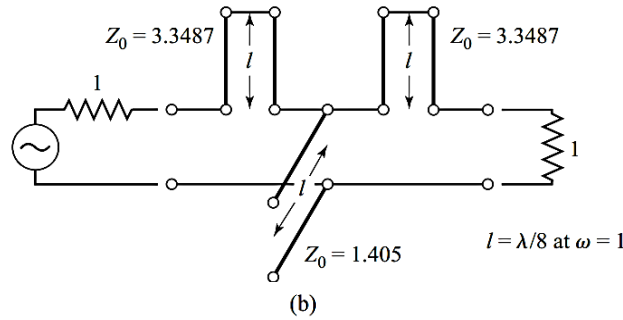
Fig 3.13. Using Richards' transformations to convert inductors and capacitors to series and shunt stubs.

The series stubs of Fig 3.12 would be very difficult to implement in microstrip line form, so we will use one of the Kuroda identities to convert these to shunt stubs. First, we add unit components at either end of the filter, as shown in Fig 3.11.

(c)
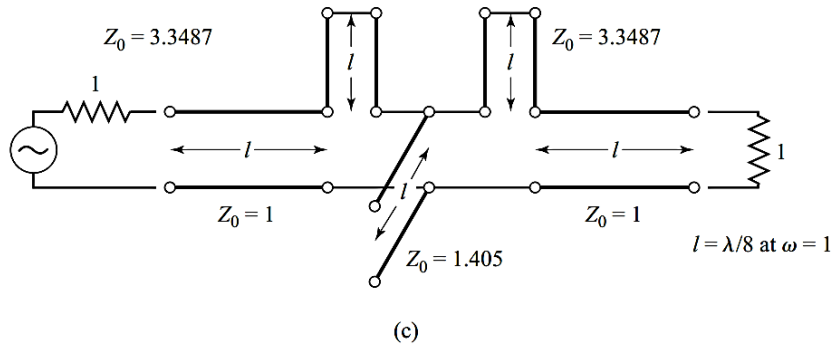
Fig 3.14. Adding unit components at the ends of the filter.

These redundant components do not affect filter performance since they are matched to the source and load ($Z_0 = 1$). Then we can apply Kuroda identity (b) from Fig to both ends of the filter. In both cases, we have that

$$n^2 = 1 + \frac{Z_2}{Z_1} = 1 + \frac{1}{3.3487} = 1.299$$

The result is shown in Fig below.

(d)
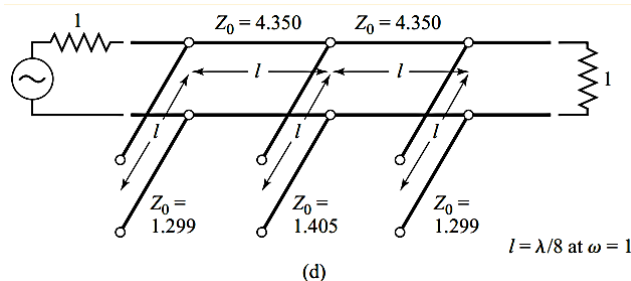
Fig 3.15. Applying the second Kuroda identity.

Finally, we impedance and frequency scale the circuit, which simply involves multiplying the normalized characteristic impedances by 50 Ω and choosing the line and stub lengths to be λ/8 at 4 GHz. The final circuit is shown in Fig 3.14,
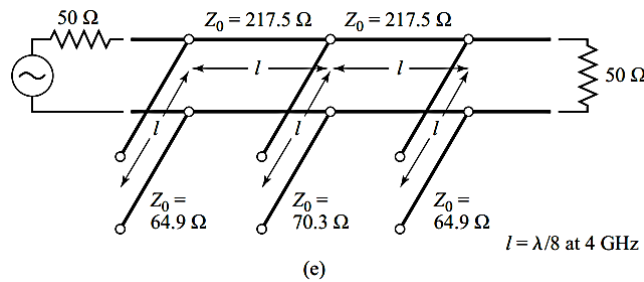
Fig 3.16. After the impedance and frequency scaling of the design.

with a microstrip layout in Fig below.
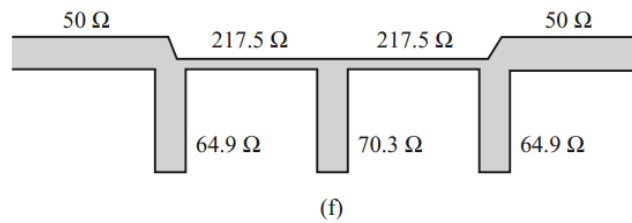
Fig 3.17. Microstrip fabrication of the final filter.

The calculated propagation response of this filter is plotted in Fig 3.15, along with the response of the lumped-element version.
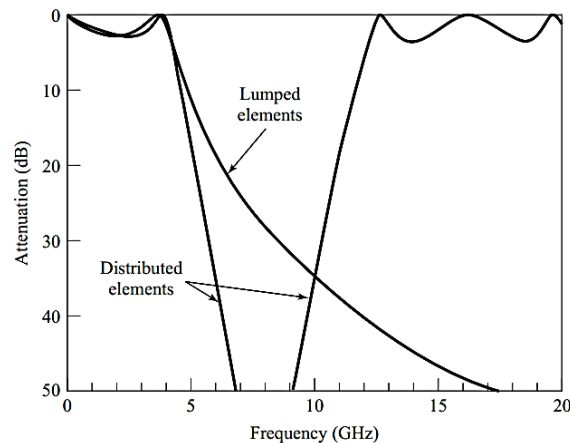
Fig 3.18. Propagation responses of lumped-element and a distributed-element LPF.

Note that the pass-band characteristics are very similar up to 4 GHz, but the distributed-element filter has a sharper cut-off. Also notice that the distributed-element filter has a response that repeats every 16 GHz, as a result of the periodic nature of Richards' transformation.

• **Stepped-Impedance LPF**

A relatively easy way to implement LPFs in microstrip or stripline is to use alternating sections of very high and very low characteristic impedance lines. Such filters are usually

referred to as stepped-impedance, or hi-Z, low-Z filters, and are popular because they are easier to design and take up less space than a similar LPF using stubs. Because of the approximations involved, however, their electrical performance is not as good, so the use of such filters is usually limited to applications where a sharp cut-off is not required.

In [57], the stepped impedance trace for crosstalk reduction was presented. Here, if the victim trace is a low-frequency or DC trace, one may employ a stepped impedance LPF configuration (i.e. using components of the alternating high and low impedance of the trace). Length l_{Hi} of the high impedance (Z_H) element can be calculated using the electrical length defined as,

$$\beta l_{Hi} = \frac{LR_0}{Z_H} \tag{3.23}$$

Where $\beta = 2\pi/\lambda$, λ corresponds to the cut-off frequency of the LPF, and R_0 illustrates the feed trace characteristic impedance. Similarly, length l_{Li} of the low impedance element (Z_L) can be calculated as,

$$\beta l_{Li} = \frac{CZ_L}{R_0} \tag{3.24}$$

where L and C are the normalized lumped element values Because of the inductors and capacitors respectively. The width of the components is chosen to correspond to impedances Z_H and Z_L. Here, Z_H and Z_L are usually set to the highest and lowest characteristic impedance values that can be practically fabricated. It is worth mentioning that the difference within the two impedances should be as high as possible for excellent filter performance (i.e. sharp cut-off). However, in this case, the sharp cut-off is not an essential requirement. Fig 3.48 illustrates an example of a 6 components LPF design. Here, Z_H = 120 Ω, Z_L = 20 Ω, and R_0 = 50 Ω, d = 0.158 cm, ϵ_r = 4.2, tan δ = 0.02 and copper conductors of 0.5 mil thickness were chosen. Also, a cut-off frequency of 2 GHz was selected. The calculated values using (4.4) and (4.5) are given in Table 3.3.
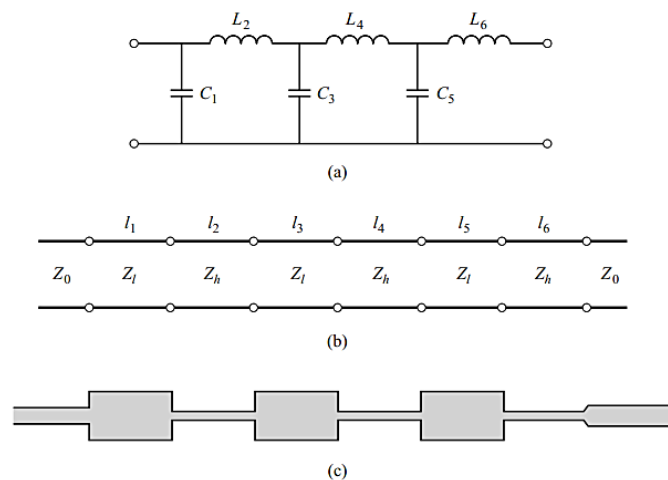
Fig 3.19. Six element (a) LPF prototype circuit. (b) Stepped-impedance implementation. (c) Microstrip layout of final filter.

Table 3.3: 6 Components Stepped Impedance LPF Design.

Element Value	Impedance (Ohm)	Electrical Length	Length (mm)	Width (mm)
$C_1=0.517$	$Z_L=20$	11.8	2.05	11.3
$L_2=1.414$	$Z_H=120$	33.8	6.63	0.428
$C_3=1.932$	$Z_L=20$	44.3	7.69	11.3
$L_4=1.932$	$Z_H=120$	46.1	9.04	0.428
$C_5=1.414$	$Z_L=20$	32.4	5.63	11.3
$L_6=0.517$	$Z_H=120$	12.3	2.41	0.428

The effect of loss is to increase the passband attenuation to about 1 dB at 2 GHz. The response of the corresponding lumped-element filter is also shown in Fig 3.17. The passband characteristic is similar to that of the stepped impedance filter, but the lumped-element filter gives more attenuation at higher frequencies. This is because the stepped-impedance filter components depart significantly from the lumped-element values at higher frequencies. The stepped-impedance filter may have other passbands at higher frequencies, but the response will not be perfectly periodic because the lines are not commensurate.
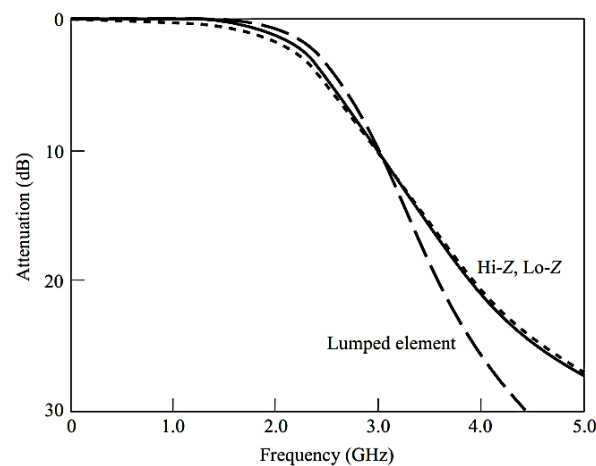
Fig 3.20. Propagation response of the stepped-impedance LPF, with (dotted line) and without (solid line) losses. The comparison with lumped-element filter is also shown in the Fig.

3.13. Conclusions

This chapter summarizes the theory of filter method in short to understand the necessity of using EBGS. Since conventional periodic structures are hold true for EBGSs, it is necessary to discuss the basic theory. Two-port networks, ABCD parameter, S-Parameter theories and image parameter and IL methods are analyzed. This chapter gives the better understanding of the phenomenon of EBGSs and wave propagation in periodic media. We investigated that the stepped impedance design is easier and better performing than stubbed LPF design but this design has higher radiated emissions as compared to the stepped impedance design. Our main purpose is to make a LPF using EBGS to reduce the complexity of the calculations and design procedure.

Chapter-4

Electromagnetic Bandgap Structures

4.1   Microstrip T-line:

The usual structure of a microstrip T-line is shown in Fig 4.1. Width (W) and thickness (t) are on the top surface of a dielectric substrate. This substrate contains a relative dielectric constant(ϵ_r) and thickness (h).
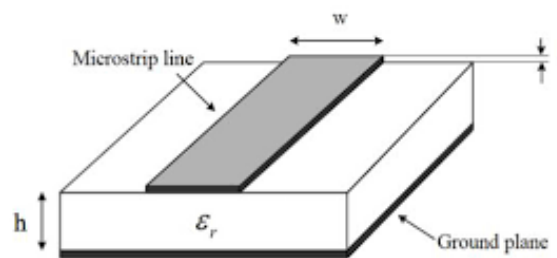
Fig 4.1: Structure of a Microstrip Tx-line.

4.2   Types and configurations of EBGSs

There are various types of Electromagnetic Bandgap Structures which are discussing below:

4.2.1 Types of Electromagnetic Bandgap Structures (EBGS):

EBGSs are periodic in nature and created by drilling, cuffing, and engraving on the dielectric substrates. They may be designed one or both side of the substrate. EBGSs are categorized as:

> (i) one dimensional (1-D),
> (ii) two dimensional (2-D)
> (iii) three dimensional (3-D) .

A periodic structure satisfies Bragg's conditions. Inter-cell separation is close to the half guided wavelength ($\lambda_g/2$), and are capable of forbidding EM propagation in various directions [51, 62].

(i) 3-D EBG Crystals:

3-D periodic dielectric structure is knows as woodpile structure which was created in ISU in the earlier stage of investigating EBGSs [4]. Its' remarkable feature is the 3-D crystals have periodicity along all the three dimensions. Though the structure has complete bandgaps, that propagation states are not allowed in any direction [52]. A good 3-D EBG structure is required to block all waves in all directions. The main limitation is to fabricate the 3-D structure is too difficult.
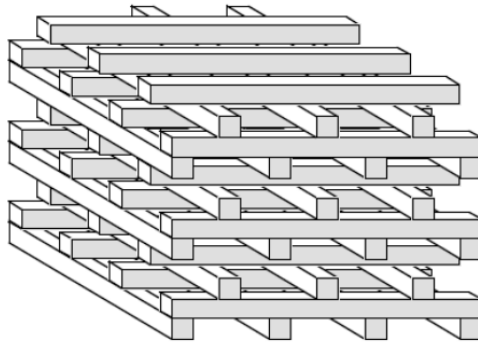
Fig 4.2: 3-D EBG structure[51]

(ii) 2-D EBG Crystals

We already learn from the literature that the fabrication is easy for 2-D EBGSs and capable of maintaining a similar control on the wave propagation in the structure as like as the 3-D structure. 2-D structures are homogeneous along the 3-D, that is all variations happen in the 2-Ds, whereas everything is constant along the 3-D, thereby propagation is allowed along one axis of the crystal [51]. These 2-D EBGSs have compactness, stability, and fabrication advantages. These advantages presented them as much attractive in recent days [52].
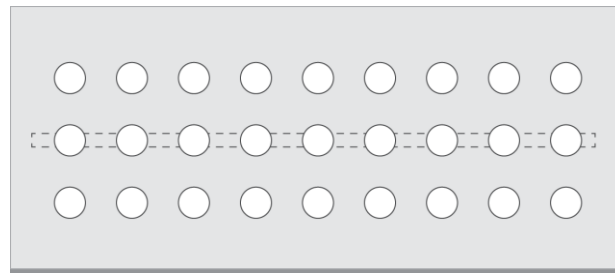
Fig 4.3: 2-D EBG structure [53, 54].

(iii) 1-D EBG Crystals

The main feature of 1-D EBG structures is the design strategy with compactness. 1-D EBGSs have the periodicity of two different media in just one direction. This basic crystal provides photonic band gaps, localized modes, and surface states. However, the limitation is only in one direction, the band gaps and bound states are limited in that direction. But this simple structure provides most of the 2-D and 3-D EBG crystal features [55].
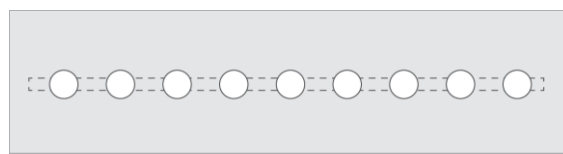
Fig 4.4: 1-D EBG structure [56].

4.2.2 EBGS Configurations

EBGSs may be formed in the ground surface or over the substrate. The T-line can also be modified to form EBG characteristics without having any perturbation in the ground surface [57-59]. Planar EBGSs and their applications to antennas have been reported in [60]. From the literature we have found the EBG configuration is categorized as shown in Fig below.
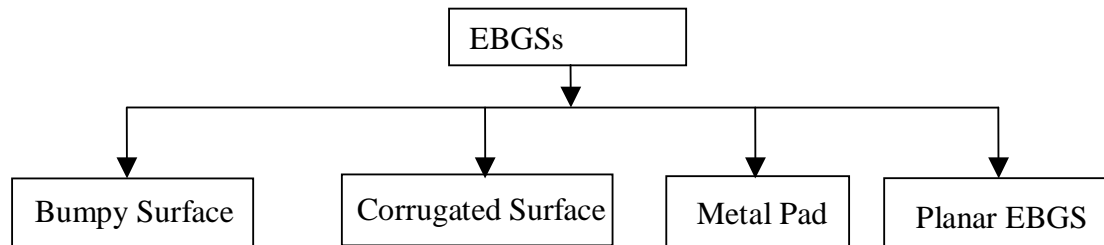
Fig 4.5: Different EBGSs

- **Bumpy Surface**

The first structure is made by drilling a periodic pattern of holes in the substrate or engraving a periodic pattern of circles in the ground surface. A bumpy metal sheet has a narrow surface wave band-gap [61-63]. Electric field wraps around the bumps at the upper edge of the band gap and the electric field also extends across the bumps at the lower edge of the band-gap, hence a slow wave structure is formed. Bumpy surface is shown in Fig below.
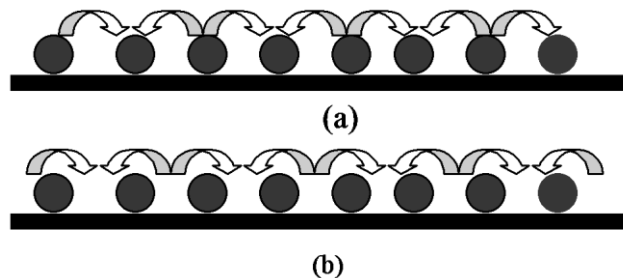
Fig 4.6: Bumpy metal sheet: (a) electric field extends across the bumps at the lower edge and (b) electric field wraps around the bumps at the upper edge

- **Corrugated Surface**

A corrugated surface is a metal slab and in this surface a series of vertical slots are cut [36], [64]. The slots are narrow so that many of them fit within one wavelength across the slab. Each slot can be regarded as a parallel plate T-line, running down into the slab, and shorted at the bottom. If the slots are one quarter-wavelength deep, then the short circuit at the bottom is transformed by the length of the slots into an open circuit at the top end. Thus the impedance at the top end is very high. In this situation, the surface impedance is capacitive and transverse magnetic (TM) surface waves are restrained. Furthermore, a plane wave polarized with the electric field perpendicular to the ridges will appear to be reflected with no phase reversal. The corrugated surface is shown in Fig below.
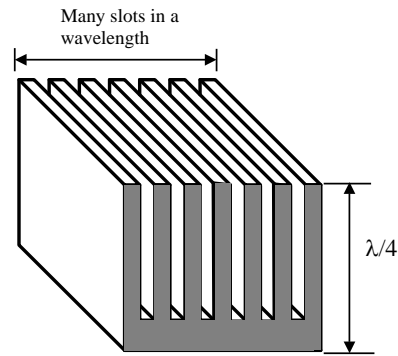
Fig 4.7: Corrugated metal surface

- **Metal Pad or High-Impedance Surface**

A more effective and compact approach, compared to the corrugated surfaces, which makes use of a triangular or square lattice of metal pads connected to ground with vias, has been recently proposed and wielded in [65] to enhance the gain of planar antennas. These structures are the first realization of planar compact electromagnetic crystals with a complete stop-band in the microwave range. This type of structure with a triangular lattice of hexagonal metal plates and square vias to the ground is shown in Fig below.
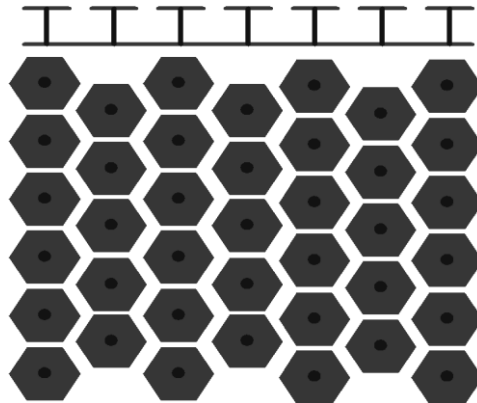
Fig 4.8: Periodic metal connected to ground via holes to yield high-impedance surface.

- **Planar EBGSs**

Planar EBGSs exhibit some interesting features such as distinctive passband and stopband, slow wave effects, low attenuation in the passband and restrainion of surface waves when serving as the ground of the planar microstrip circuit. Several Planar EBG configurations have been reported in the literature like uni-planar designs without vertical vias, one and two-dimensional EBG T-line design, etc. in which they used EBG basis points with different geometries, and shapes like circular shape, square, hexagonal, fork shape, plus sign and many more. In some planar devices, they create defects by creating a discontinuity in a periodic pattern. For example, in a planar circular defect induced EBG structure with triangular lattice, they remove some circles or change their size for creating some discontinuity.
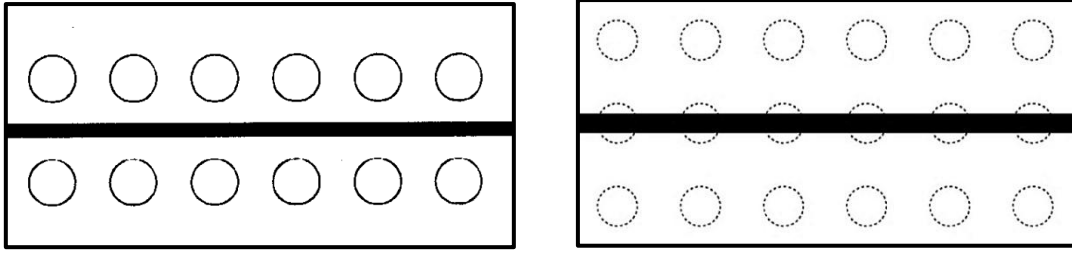
Fig 4.9: Microstrip with the engraved circular pattering in the ground surface [50]

4.3 Analysis methods for Triangular Dumbbell-shaped DGSs

The center frequency of the stop-band of an EBG is on an average calculated by Bragg's condition [60]. Using this formula, the period for any stop-band frequency can be determined. At DGS, the dimensions of the dumbbell-shaped DGS unit cell control the current paths on the ground surface hence the equivalent inductance and capacitance of the ground. Triangular dumbbell shaped DGS is structured by two larger triangular slots connected by a narrow vertical slot. On the other hand, the narrower vertical slot is a rectangular pattering EBG element.
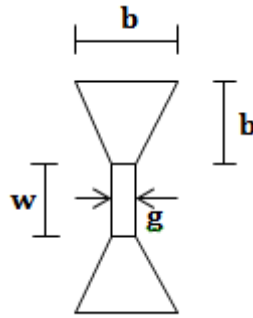
Fig 4.10: Graphical representation of a unit cell of a triangular dumbbell shape DGS.

The arm length of a larger triangular pattering slot is 'b'. The vertical rectangular slot has the width, w and gap g. The unit cell is engraved in the ground surface of a standard 50Ω T-line. In order to investigate the frequency characteristics of the unit DGS cell, few structures having different width and gaps sizes are simulated. We can be expressed the larger slot as an inductor and the narrower slot as a capacitor and also expressed similar as a electric circuit. The lumped LC equivalent model can be expressed as [33]:

$$C = \frac{\omega_c}{Z_0 g_1}\left[\frac{1}{\omega_0^2 - \omega_c^2}\right] \tag{4.1}$$

$$L = \frac{1}{4\pi^2 f_0^2 C} \tag{4.2}$$

Where f_0 is the frequency of the attenuation pole, ω_c is the angular cut-off frequency, Z_0 is the characteristic impedance of the line, and g_1 is the admittance value of the Butterworth LPF response. The equivalent circuit of the DGS unit cell is shown in Fig below.
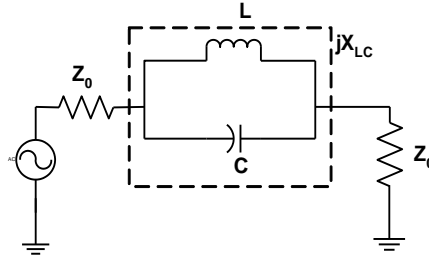
Fig 4.11:   The equivalent circuit of the triangular dumbbell-shaped DGS unit.

4.4   Design Equations of Microstrip T-line over Uniform EBGS:

The investigation is concentrated into only on EBG assisted microstrip T-line. Commercially available software tool Zealand IE3D will be used to design and to extract S-Parameters for all designs due to the flexibility of Zealand IE3D. Zealand IE3D is a method of moment (MOM) based full-wave analysis tool, hence very accurate. The perturbation in the ground surface in the form of EBGS creates stopband that is useful for spurious transmission and to improve the performance of antennas, filter, and other microwave devices and components.

In this section, it is a conventional rule to use Bragg's condition to calculate the central stopband frequency provided by EBGSs [60]. Under this condition Because of the inter-cell separation, the size of the EBG element is calculated on the basis of Filling factor (FF). The Graphical representation of the design is pattering under 50Ω T-line are designed by using "Taconic Substrate" in which relative dielectric constant $\varepsilon_r = 2.45$, Thickness, h=31mil or 0.787mm. Personal Computer Aided Antenna Design 5.0 (PCAAD) software is used Because of the values of T-line where, width, w = 0.2263cm and effective dielectric constant, $\varepsilon_{eff} = 2.068$ has been found.

We know that,

$$\lambda_0 = \frac{300 \ (mm)}{f_c \ (GHz)} \tag{4.3}$$

$$\lambda_g = \frac{\lambda_0}{\sqrt{\varepsilon_{eff}}} \tag{4.4}$$

$$a = \frac{\lambda_g}{2} \tag{4.5}$$

Now,

$$a = \frac{\lambda_g}{2} = \frac{20.88}{2} = 10.44 \ mm$$

Filling factor, $\text{FF} = \frac{r}{a}$ (4.6)

Where,

r = radius of circular EBGS,

a = inter-element spacing.

The center frequency of the stopband is calculated on an average with the following expression:

$$\beta a = \pi \tag{4.7}$$

Where 'a' is the inter-cell separation of the EBG pattern, and β is the wave number in the dielectric slab and is defined by the expression:

$$\beta = \frac{2\pi f_0}{c}\sqrt{\varepsilon_{eff}} \tag{4.8}$$

Where,

f_0 = the center frequency of the stop-band

ε_{eff} = the effective relative permittivity of the dielectric slab

c = the speed of light in free space

For example, $f_c = 10\ GHz$,

$$\lambda_0 = \frac{300}{10} = 30\ mm$$

$$\lambda_g = \frac{\lambda_0}{\sqrt{\varepsilon_{eff}}} = \frac{30}{2.068} = 20.88\ mm$$

4.5   Designs of Uniform EBGSs:

The following different microstrip T-lines are designed. All the EBGSs are designed at the stop-band central frequency of 10 GHz.

- **Standard 50 Ω T-line:**

A standard 50 Ω line is realized on Taconic substrate having a dielectric constant of 2.45 and height of 31 mils.

(a)

(b)
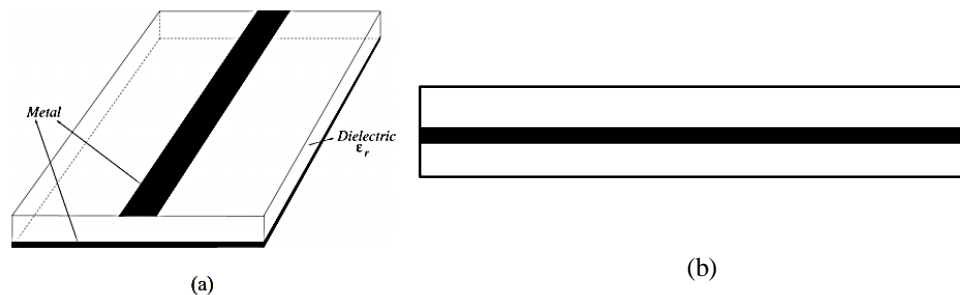
Fig 4.12: Microstrip T-line: (a) 3D view; (b) 2D view.

- **S-Parameter result of the ideal T-line:**

The S-Parameters of the designs have been investigated of 50Ω T-line. The Taconic substrate is used in the simulation Because of the ideal and uniform structured EBGSs. The simulated S-Parameter performances of an ideal T-line are shown in Fig below. The IL is on an average zero dB throughout the whole frequency range from 0 to 14 GHz.
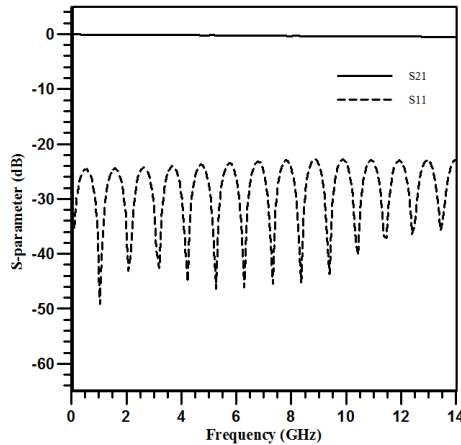
Fig 4.13: IE3D simulated S-Parameters versus frequency of an ideal 50 Ω T-line. The substrate is Taconic having the height of 31 mils and the dielectric constant is 2.45

- **2-D uniform circular components in the ground surface:**

This design gives the idea of the optimum value of FF to be 0.25. The inter-element spacing, a= 10.44 mm, radius, r = 2.6075 mm. The Graphical representation of a three rows (2-D) uniform hole pattering EBGSs in the ground surface of a 50 Ω T-line is shown in Fig.
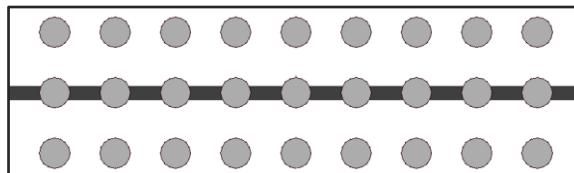
Fig 4.14: Graphical representation of a 50 Ω microstrip T-line where 2-D uniform circular EBGSs are engraved in the ground surface.

- **1-D uniform circular EBGSs in the ground surface:**

This design is to consider 1-D EBGSs that replace 2-D EBGSs. The Graphical representation of the 1-D uniform circular pattering EBGSs is shown in Fig. In this design, only one row of EBG components is engraved in the ground surface just under the 50 Ω T-line. The inter-element spacing, a= 10.44 mm, radius, r = 2.6075 mm.
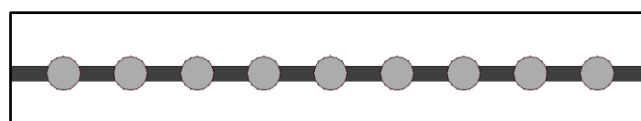
Fig 4.15: Graphical representation of a standard 50 Ω T-line with 1-D uniform circular EBGSs engraved in the ground surface.

- **S-Parameter result of the T-line with 2-D Uniform Circular EBGS**

The S-Parameters of the designs have been investigated of 50Ω T-line. The Taconic substrate is used in the simulation Because of the ideal and uniform structured EBGSs. The radius of the each uniform circular EBGS is 2.6075 mm and the inter element gap is 10.44 mm. S-Parameter performance of a 2-D uniform circular EBGS is shown in the Fig below.
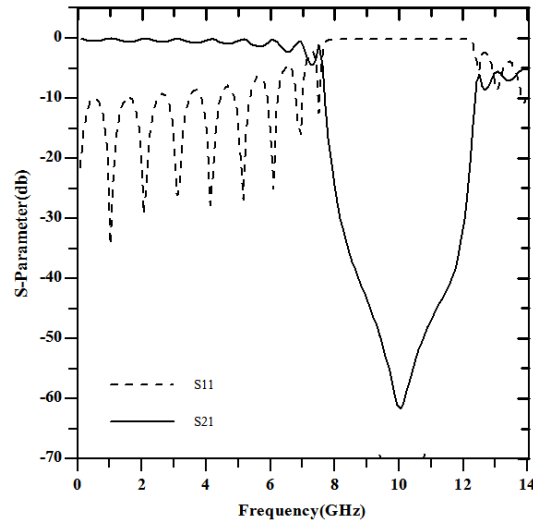
Fig 4.16: Simulated S-Parameter performances of a standard 50 Ω T-line perturbed by 2-D (three lines) uniform circular EBGSs in the ground surface.

We have seen that, the 10 dB RL bandwidth is 7.3 GHz; the 20 dB rejection bandwidth is 4.3 GHz. Around cut-off frequencies, ripples are observed. The center frequency is found to be shifted around 10.06 GHz. The maximum value of isolation is found to be 64 dB.

- **S-Parameter result of the T-line with 1-D Uniform Circular EBGSs**

The optimum FF for Taconic substrate is 0.25 with a dielectric constant of 2.45 and height of 31 mils. Based on this value a microstrip T-line with 1-D uniform circular EBGSs has also been investigated. S-Parameter performance of a 1-D uniform circular EBGS is shown in the Fig below.

Fig 4.17: Simulated S-Parameter performances of a standard 50 Ω T-line perturbed by 1-D (one line) uniform circular EBGSs in the ground surface.

It can be seen that the maximum isolation is found to be 59.46 dB. The 10 dB RL bandwidth is 7.4 GHz; the 20 dB rejection bandwidth is 4.8 GHz. Around cut-off frequencies, ripples are observed. The center frequency is found to be shifted around 10.06 GHz.

From S-Parameter performances of 2-D and 1-D design, it is very clear that 1-D EBGSs and 2-D EBGSs provide very similar performances.

- **Designs of Uniform Square Pattering EBGSs**

Uniform square pattering EBGSs will also be designed. Here three rows and one row EBGSs will be designed and their performances will be compared. It will be useful to replace three rows EBGSs by 1-D EBGSs. On the basis of the availability of the materials Because of the fabrications Taconic substrate with ε_r = 2.45 and height (h) = 31 mils is used in the simulation.

1. **2-D Uniform Square Pattering EBGSs:**

The conventional uniform square pattering EBGSs are shown in Fig 4.18. Three lines of total 27 EBG components are engraved under the standard 50 Ω T-line. The FF is taken to be 0.5. The substrate is Taconic having a dielectric constant of 2.45 and height of 31 mils.

Fig 4.18: 2-D (three lines) of square pattering EBGSs beneath standard 50 Ω T-line.

2. **1-D square pattering EBGSs:**

The Graphical representation of 1-D (one line) circular pattering EBGSs is shown in Fig 4.19. Total 9 EBG components are engraved under the standard 50 Ω T-line. The FF is taken to be 0.5. The substrate is Taconic having a dielectric constant of 2.45 and height of 31 mils.

Fig 4.19: 1-D square pattering periodic structures under a standard 50 Ω T-line.

- **S-Parameter result of the T-line with 2-D Uniform rectangular EBGSs**

The S-Parameter performances of uniform square pattering EBGSs have been investigated. The inter-element spacing is 10.44 mm and FF is 0.5. The simulated and measured S-Parameter performances of three lines (2-D) uniform square pattering EBGSs are shown in Fig below.

Fig 4.20: S-Parameter performances of three lines uniform square-pattering EBGSs.

It can be seen from the Fig that this design provides wider pass-band and deeper stop-band. The 20 dB IL bandwidth is 5.5 GHz. The ripple height along the pass-band is negligible. The center frequency is found to be shifted around 10.6 GHz. The maximum value of isolation is found to be 54dB.

- **S-Parameter result of the T-line with 1-D Uniform rectangular EBGSs**

Based on the value a microstrip T-line with 1-D uniform rectangular EBGSs has been investigated. The simulation result is shown in Fig. 4.21.
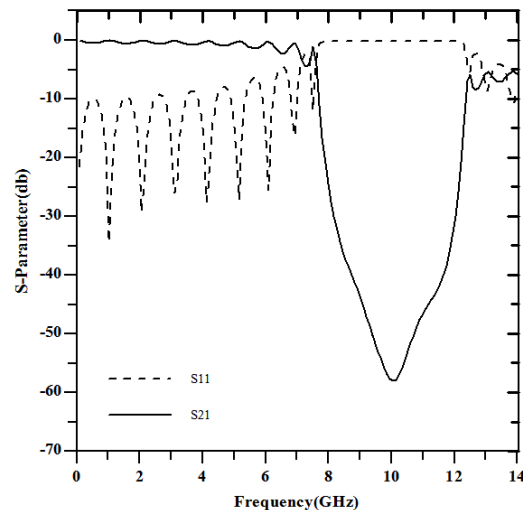
Fig 4.21: Simulated S-Parameter performances of a standard 50 Ω T-line perturbed by 1-D (one line) uniform rectangular EBGSs in the ground surface.

From the Fig it can be seen that RL performance, stopband characteristics and ripple height for this design are similar to 2-D design. One row of uniform rectangular EBGS provides on an average 59.5 dB altitude. The 20 dB IL bandwidth is 5.5 GHz and center frequency is as like as 2-D uniform rectangular EBGS.

From S-Parameter performances of 2-D and 1-D design, it is very clear that 1-D EBGSs and 2-D EBGSs provide very similar performances.

- **Designs of Uniform Triangular Pattering EBGSs**

Uniform triangular pattering EBGSs will also be designed. Here three rows and one row EBGSs will be designed and their performances will be compared. It will be useful to replace three rows EBGSs by 1-D EBGSs. On the basis of the availability of the materials Because of the fabrications Taconic substrate with $\varepsilon_r = 2.45$ and height (h) = 31 mils is used in the simulation.

1. 2-D Uniform Triangular Pattering EBGSs:

The conventional uniform triangular pattering EBGSs are shown in Fig 4.22. Three lines of total 27 EBG components are engraved under the standard 50 Ω T-line. The FF is taken to be 0.5.
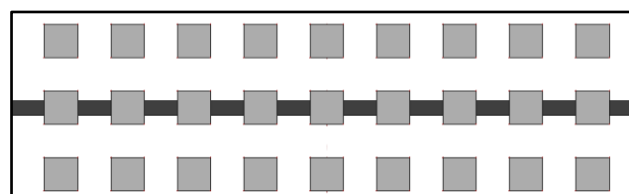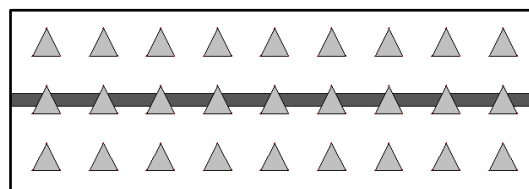

Fig 4.22:   2-D (three lines) of triangular pattering EBGSs beneath standard 50 Ω T-line.

2. 1-D triangular pattering EBGSs:

The Graphical representation of 1-D (one line) triangular pattering EBGSs is shown in Fig 4.23. Here only 9 EBG components are engraved in the ground surface.
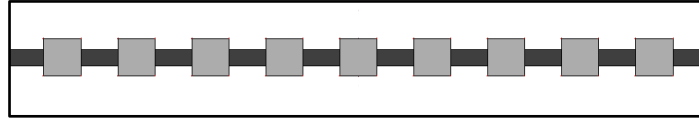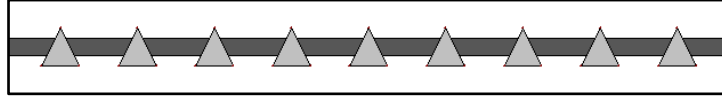

Fig 4.23: 1-D triangular pattering periodic structures under a standard 50 Ω T-line.

- **S-Parameter result of the T-line with 2-D Uniform triangular EBGSs**

The S-Parameter performances of uniform triangular pattering EBGSs have also been analyzed. The simulated and measured S-Parameter performances of three lines (2-D) uniform triangular pattering EBGSs are shown in Fig 4.24.
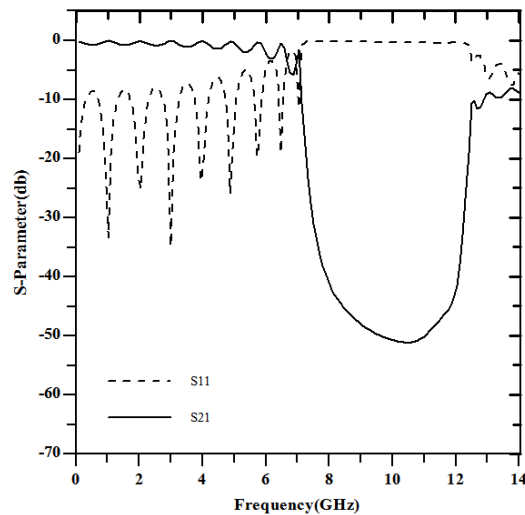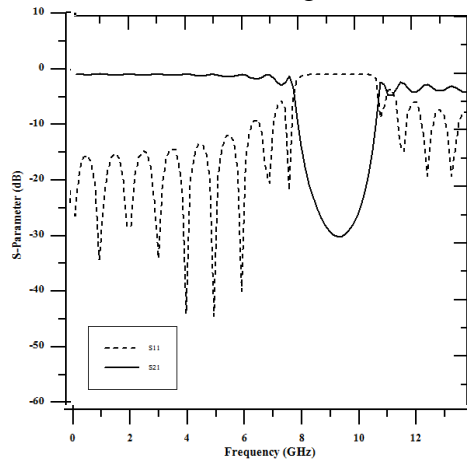

Fig 4.24: S-Parameter performances of three lines uniform triangular pattering EBGSs.

It can be seen from the Fig that this design provides pass-band and stop-band like circular designs. The 20 dB rejection bandwidth is 8.12 GHz. The ripple height along the pass-band is negligible. But around cut-off frequencies, ripples are observed. The center frequency is found to be shifted around 9.6 GHz resulting in 4% frequency deviations from the design frequency. The maximum value of isolation is found to be 30 dB.

- **S-Parameter result of the T-line with 1-D Uniform triangular EBGSs**

It is mentioned that 0.5 is the optimum FF for Taconic with a dielectric constant of 2.45 and height of 31 mils. Based on this value a microstrip T-line with 1-D uniform triangular EBGSs has also been investigated. The simulation result is shown in Fig. 4.25.
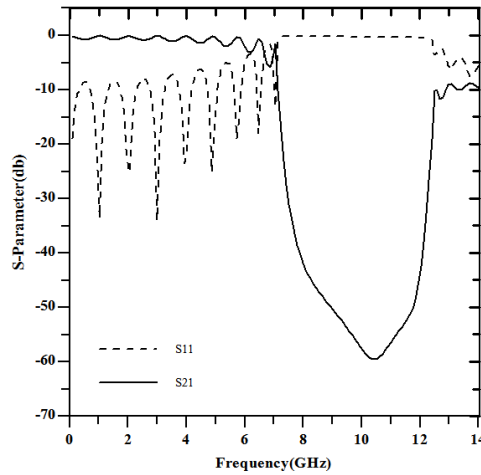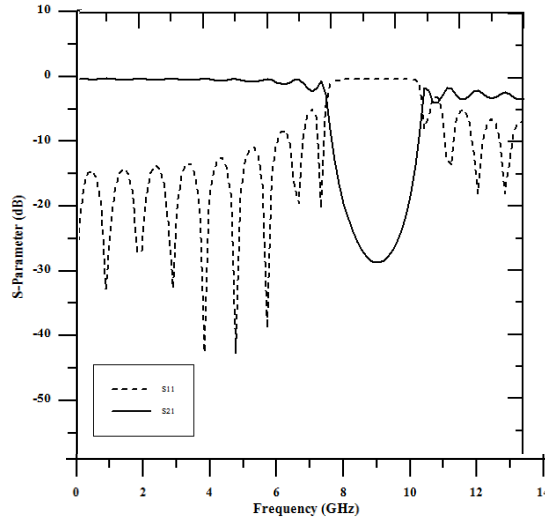
Fig 4.25: S-Parameter performances of one lines uniform triangular pattering EBGSs.

From the Fig. 4.25, it can be seen that RL performance, stopband characteristics and ripple height for this design are similar to 2-D design. A small difference in the value of maximum isolation is observed. In the case of three rows of uniform rectangular EBGSs, the maximum isolation is found to be on an average 31.1 dB. On the other hand, one row of uniform rectangular EBGS provides on an average 30 dB.

4.6 Designs of Uniform EBGSs Using the Same Area

Some 1-D uniform circular, rectangular and triangular pattering EBGSs with same areas will be designed. In the design, the radius of circular EBGS is r = 2.6075 mm is taken. So, for taking the similar area of different types of EBGS, the arm of a rectangular EBGS will be calculated as well as triangular EBGS.

Here, the area of a circular EBGS= πr^2 (4.9)

Area of rectangular EBGS = b^2 (4.10)

Area of triangular EBGS = $\frac{1}{2}c^2$ (4.11)

So, $b = \sqrt{\pi r^2} = \sqrt{\pi \times 2.6075^2} = 4.6216$ mm

And, $c = \sqrt{2\pi r^2} = \sqrt{2 \times \pi \times 2.6075^2} = 6.536$ mm
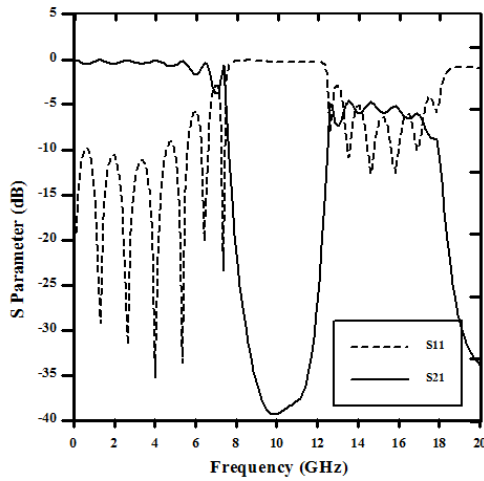
10 dB RL BW= 7.5 GHz
20 dB IL BW= 3 GHz
Passband Ripple Height= 4 dB

Fig 4.26: S-Parameter performance of one line uniform circular EBGSs in a certain area.
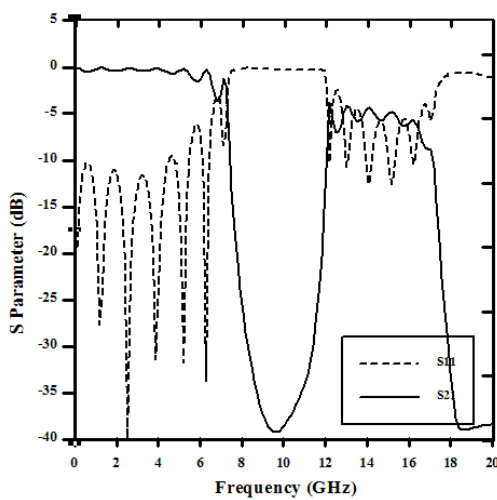
10 dB RL BW= 6.3 GHz
20 dB IL BW= 3.5 GHz
Passband Ripple Height= 4 dB

Fig 4.27: S-Parameter performance of one line uniform rectangular EBGSs of same area of circular EBGS.
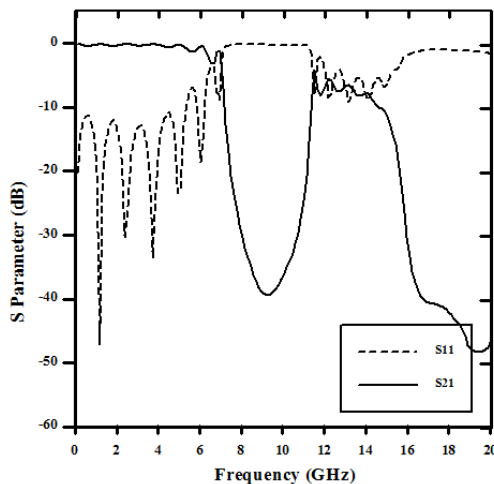
10 dB RL BW= 5.8 GHz
20 dB IL BW= 4 GHz
Passband Ripple Height= 4 dB

Fig 4.28: S-Parameter performance of one line uniform triangular EBGSs of same area of circular EBGS.

These designs are done with the circular, rectangular and triangular EBGSs of same areas. From this table we could conclude that size does not matter for different EBGSs pattern of same areas.

4.7   Uniform Circular EBGSs using different FFs

1-D uniform circular pattering EBGSs with different filling factor will be designed and their performances will be compared. The S-Parameter performances of uniform circular pattering EBGSs using different filling factor have also been analyzed. On the basis of the availability of the materials Because of the fabrications Taconic substrate with ε_r = 2.45 and height = 31 mils is used in the simulation has shown in Fig below.
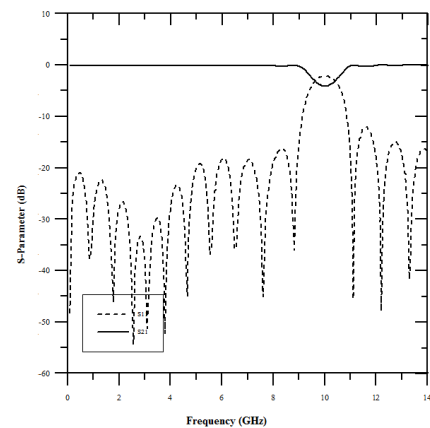
10 dB RL BW= 2.1 GHz
20 dB Rejection Loss BW= 0 GHz
Passband Ripple Height= 0 dB

Fig 4.29:   Geometry and simulation result of a standard 50 Ω T-line with 1-D uniform circular EBGSs engraved in the ground surface with 0.1 filling factor. The inter-element spacing, a= 10.44 mm.
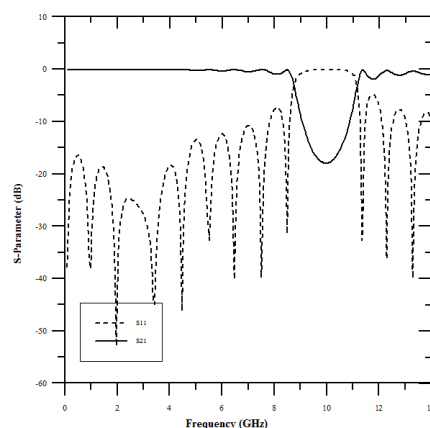
10 dB RL BW= 3.4 GHz
20 dB Rejection Loss BW= 0 GHz
Passband Ripple Height= 1 dB

Fig 4.30:   Geometry and simulation result of a standard 50 Ω T-line with 1-D uniform circular EBGSs engraved in the ground surface with 0.15 filling factor. The inter-element spacing, a= 10.44 mm.
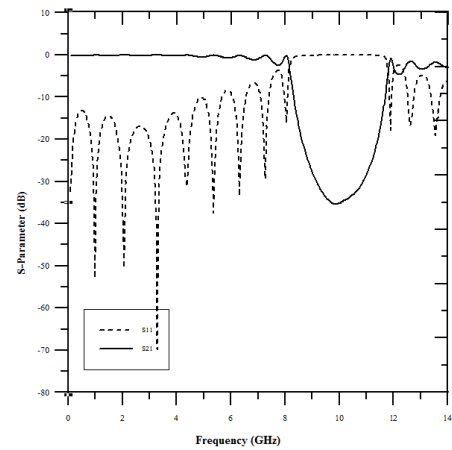
10 dB RL BW= 3.8 GHz
20 dB Rejection Loss BW= 2.8 GHz
Passband Ripple Height= 2 dB

Fig 4.31: Geometry and simulation result of a standard 50 Ω T-line with 1-D uniform circular EBGSs engraved in the ground surface with 0.2 filling factor. The inter-element spacing, a= 10.44 mm.
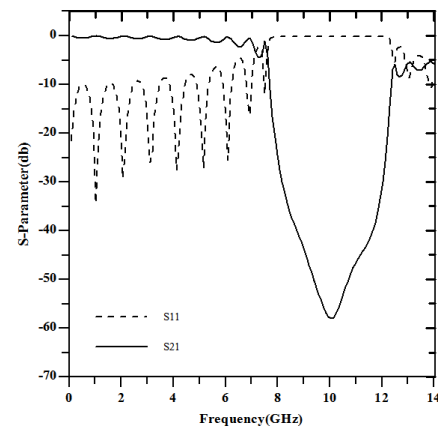
10 dB RL BW= 4.7 GHz
20 dB Rejection Loss BW= 5.2 GHz
Passband Ripple Height= 4 dB

Fig 4.32: Geometry and simulation result of a standard 50 Ω T-line with 1-D uniform circular EBGSs engraved in the ground surface with 0.25 filling factor. The inter-element spacing, a= 10.44 mm.
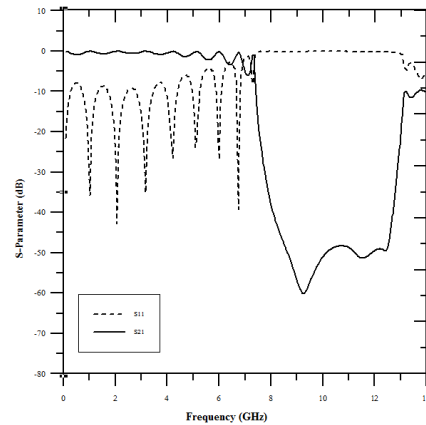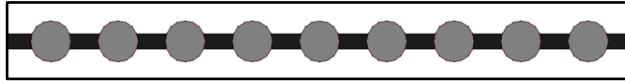
10 dB RL BW= 7.5 GHz
20 dB Rejection Loss BW= 5.8 GHz
Passband Ripple Height= 6 dB

Fig 4.33: Geometry and simulation result of a standard 50 Ω T-line with 1-D uniform circular EBGSs engraved in the ground surface with 0.3 filling factor. The inter-element spacing, a= 10.44 mm.
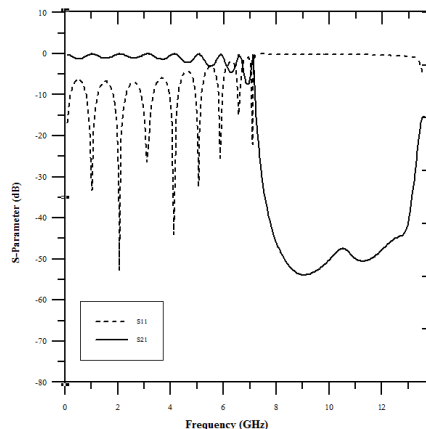
10 dB RL BW= 8 GHz
20 dB Rejection Loss BW= 6.4 GHz
Passband Ripple Height= 7 dB

Fig 4.34: Geometry and simulation result of a standard 50 Ω T-line with 1-D uniform circular EBGSs engraved in the ground surface with 0.35 filling factor. The inter-element spacing, a= 10.44 mm.

4.8 Uniform Rectangular EBGSs Using Different EBG Number

Here Uniform circular DGS has been designed with the different number over the T-line to test the improvement of the filter. Here it has been shown that the range of EBGS numbers that will give better simulation result of good insertion and RL. The EBGSs dimension is (205 x 205) mils and inter-element spacing is 411 mils. We would conclude that EBGSs of range 5 to 10 has given the best performance. So this range will be a follower for our further research.
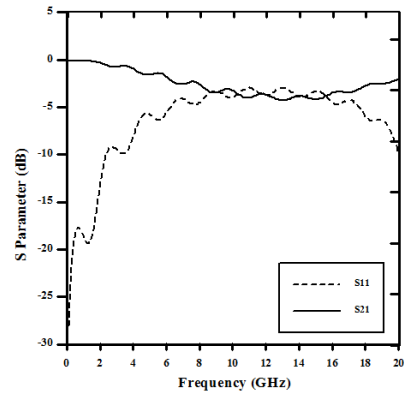
10 dB RL BW= 2 GHz
20 dB Rejection Loss BW= n/a
Passband Ripple Height= 4.5 dB

Fig 4.35: Simulated S-Parameter performance of one dimensional (one line) uniform rectangular 1 EBGSs engraved over the ground surface.
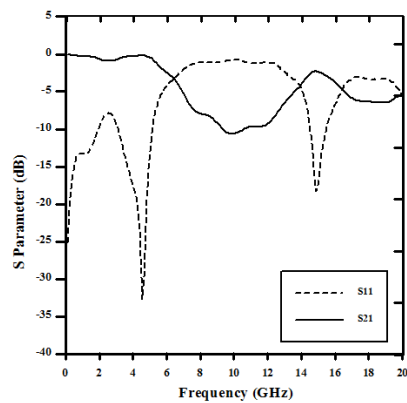
10 dB RL BW= 5 GHz
20 dB Rejection Loss BW= n/a
Passband Ripple Height= 1 dB

Fig 4.36: Simulated S-Parameter performance of one dimensional (one line) uniform rectangular 2 EBGSs engraved over the ground surface.
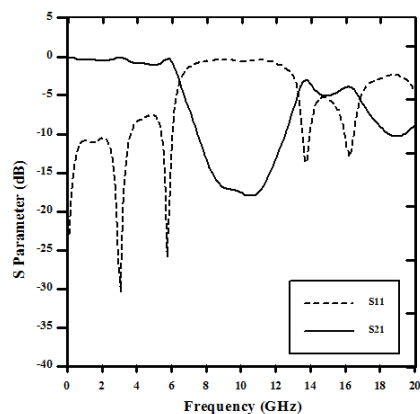
10 dB RL BW= 6 GHz
20 dB Rejection Loss BW= n/a
Passband Ripple Height= 1.5 dB

Fig 4.37: Simulated S-Parameter performance of one dimensional (one line) uniform rectangular 3 EBGSs engraved over the ground surface.
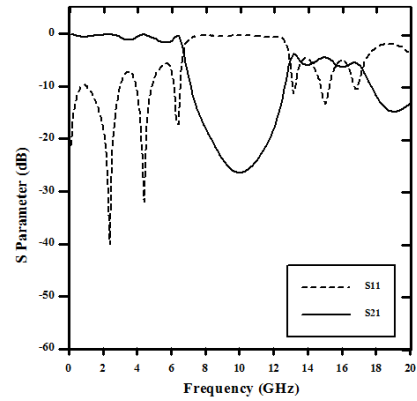
10 dB RL BW= 6.4 GHz
20 dB Rejection Loss BW= 3.6 GHz
Passband Ripple Height= 1.8 dB

Fig 4.38: Simulated S-Parameter performance of one dimensional (one line) uniform rectangular 4 EBGSs engraved over the ground surface.
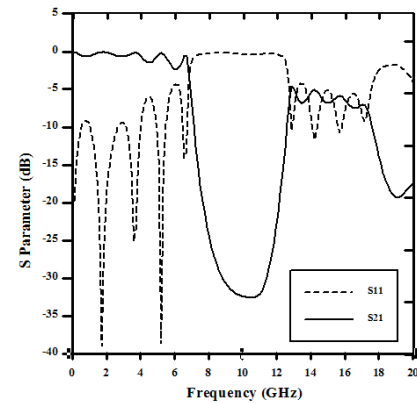
10 dB RL BW= 6.8 GHz
20 dB Rejection Loss BW= 3.1 GHz
Passband Ripple Height= 2.4 dB

Fig 4.39: Simulated S-Parameter performance of one dimensional (one line) uniform rectangular 5 EBGSs engraved over the ground surface.
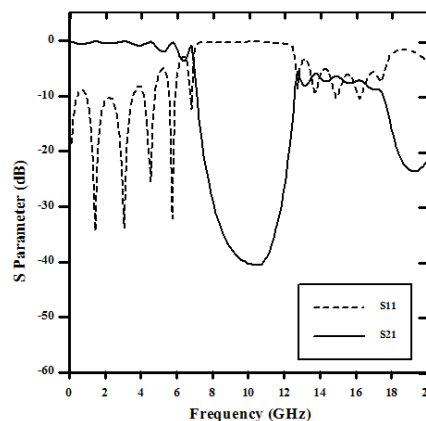
10 dB RL BW= 6.4 GHz
20 dB Rejection Loss BW= 5.1 GHz
Passband Ripple Height= 3.6 dB

Fig 4.40: Simulated S-Parameter performance of one dimensional (one line) uniform rectangular 6 EBGSs engraved over the ground surface.
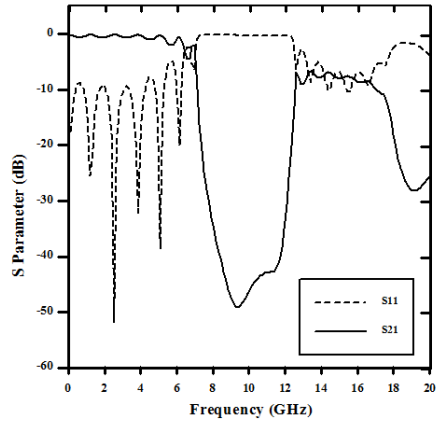
10 dB RL BW= 6.2 GHz
20 dB Rejection Loss BW= 5.4 GHz
Passband Ripple Height= 4.6 dB

Fig 4.41: Simulated S-Parameter performance of one dimensional (one line) uniform rectangular 7 EBGSs engraved over the ground surface.
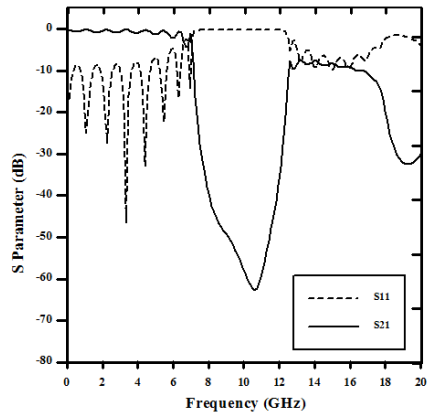
10 dB RL BW= 6.8 GHz
20 dB Rejection Loss BW= 5.5 GHz
Passband Ripple Height= 5 dB

Fig 4.42: Simulated S-Parameter performance of one dimensional (one line) uniform rectangular 8 EBGSs engraved over the ground surface.
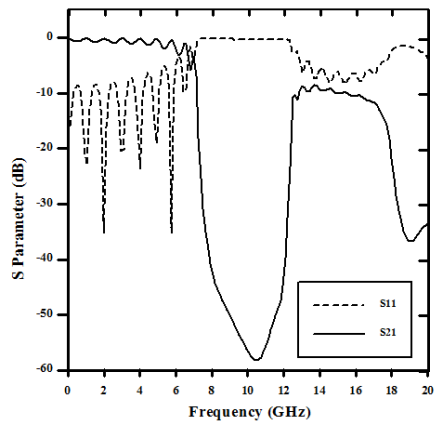
10 dB RL BW= 6.8 GHz
20 dB Rejection Loss BW= 5.5 GHz
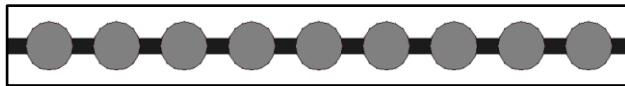Passband Ripple Height= 5 dB

Fig 4.43: Simulated S-Parameter performance of one dimensional (one line) uniform rectangular 9 EBGSs engraved over the ground surface.
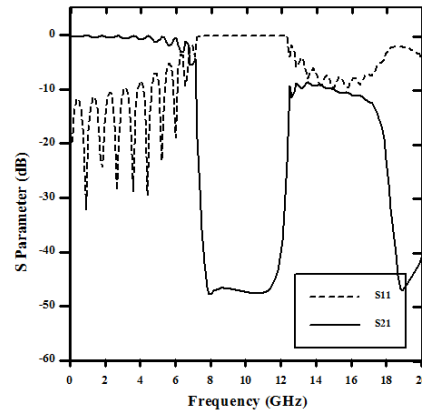
10 dB RL BW= 6GHz
20 dB Rejection Loss BW= 5.3 GHz
Passband Ripple Height= 5.5 dB

Fig 4.44: Simulated S-Parameter performance of one dimensional (one line) uniform rectangular 10 EBGSs engraved over the ground surface.

4.9 Designs of Uniform Dumbbell-shaped Defected Ground Structures (DGSs)

Uniform dumbbell-shaped DGSs will also be designed. Here one row dumbbell-shaped DGSs will be designed. On the basis of the availability of the materials Because of the fabrications Taconic substrate with ε_r = 2.45 and height (h) = 31 mils is used in the simulation. The bigger slot dimension is 205×205 mils and narrow slot dimension is 50×200 mils.

- **1-D Dumbbell-shaped DGSs**

The Graphical representation of 1-D Dumbbell-shaped DGS is shown in Fig below. Here only ten DGS components are engraved in the ground surface. The substrate is Taconic having a dielectric constant of 2.45 and height of 31 mils. The inter-element spacing is 10.44 mm.
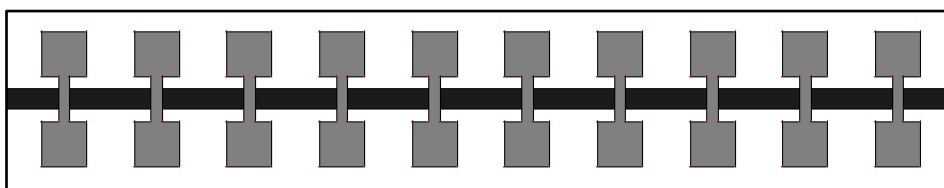
Fig 4.45: 1-D Dumbbell-shaped DGSs pattering periodic structures under a standard 50 Ω T-line.

The simulation result is shown below
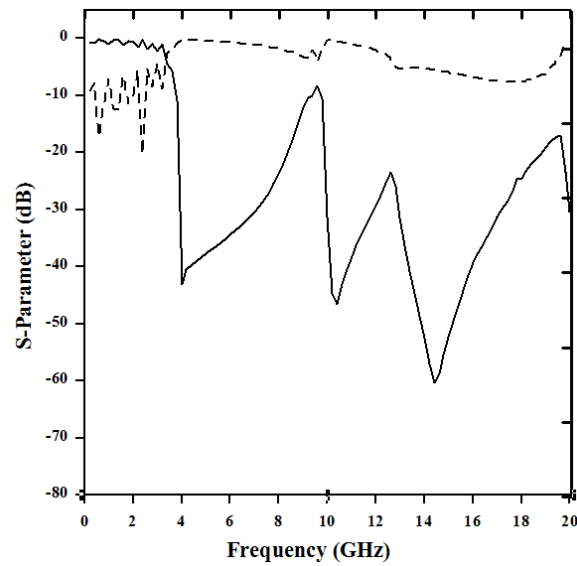
Fig 4.46: S-Parameter performances of three lines uniform Dumbbell-shaped DGS structures.

It can be seen from the Fig that this design provides narrower passband. The 20 dB rejection bandwidth is 4 GHz. The maximum value of isolation is found to be 62 dB.

4.10 Compactness of DGSs over conventional EBGSs

DGS plays a vital role to make the compact size structures. Fig 4.47 is the design of the square pattering 1-D EBG structure. The change is that, the filling factors i.e., the interval within two EBGSs are increased.
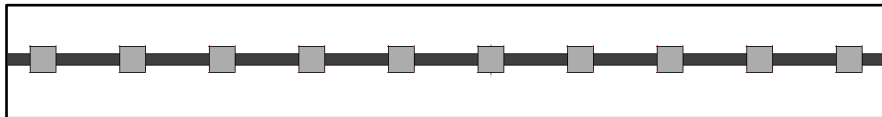
Fig 4.47: 1-D square pattering periodic structures under a standard 50 Ω T-line. The substrate is Taconic having a dielectric constant of 2.45 and height of 31 mils.

The Graphical representation of the IL performances of a standard 50Ω T-line perturbed by 1-D (one line) uniform rectangular EBGSs vs. Dumbbell-shaped DGS is shown below,
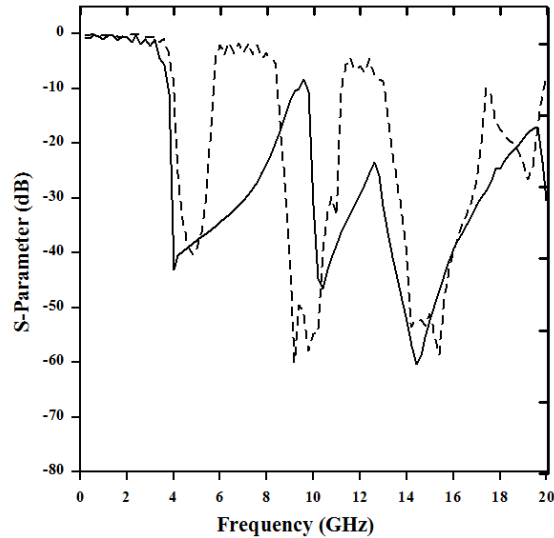
Fig 4.48: Simulated IL performances of a standard 50 Ω T-line perturbed by 1-D (one line) uniform rectangular EBGSs vs. Dumbbell-shaped DGS in the ground surface.

Usually, the conventional square pattering 10 uniform EBGSs beneath the T-line with regular periodic structure makes the center frequency near about 10 GHz and cut-off frequency near about 7 GHz. But if we double the inter element spacing, we get the cut-off frequency near about 4 GHz. But this increases the total size of the structure. This is the main drawback of the conventional EBGSs. On the other hand Dumbbell shaped DGS reaches the similar cut-off frequency with the usual inter-element spacing (10.44 mm). Stopband is not wide as Dumbbell shaped DGS in conventional structures. Analyzing above Fig, a thing is clear that DGSs are miniaturized the total designs and give the significant performance.

4.11   Conclusion

Firstly, the T-line model has been presented. To understand the properties of EBGSs the theory of EBGSs and dumbbell-shaped DGS structures has been presented in short extent. Since they are also periodic in nature all theories of periodic structures hold true for EBGSs.

Uniform circular, square-shaped EBGSs and dumbbell-shaped DGSs have been analyzed. All designs have been investigated with FF of 0.25 for circular EBGSs and 0.5 for both rectangular EBGSs and dumbbell-shaped DGSs is considered to be the optimum value of FF. Three rows and one row uniform EBGSs are studied to replace 2-D EBG components by 1-D EBG components for both the shapes. Both the designs provide very similar performances. Finally, we could conclude that it is preferred to use 1-D EBGSs rather than 2-D EBGSs and for better results, we could use dumbbell shape structures.

Chapter-5

EBG Assisted T-line for LPF

5.1 Introduction

In previous chapter, conventional EBGSs with optimum FFs and the optimal numbers of EBG structured components and dumbbell-shaped DGSs have been investigated. We found that, passband ripples and low bandwidth in bandstop portion are the two serious problems of conventional uniform EBGSs. But Uniform DGS could solve some of those problems. In this chapter non-uniform EBGSs will be investigated. The periodicity of the non-uniform structure is realized by non-uniform distribution. Here, DGSs in the form of non-uniform distributions of different patterns are proposed to investigate the improvement in S-Parameter performance. The non-uniform distributions and with hybrid designs have performed exclusive performances by restraining passband ripples and wide stopbands. Hence the filter synthesis is appreciably relaxed in the present strategy. Also, the altitude of passband RL, selectivity, and the ripples can be controlled with the non-uniform patterns.

5.2 Theory of Binomial Distribution

This theory is the imposition of the probability distribution Because of the discrete number of successes in an independent sequence of experiments. This distribution is determined by the polynomial equation. The coefficients of the polynomial are:

$$(1 + x)^{m-1} = 1 + (m - 1)x + \frac{(m - 1)(m - 2)}{2!}x^2 \quad + \frac{(m - 1)(m - 2)(m - 3)}{3!}x^3 + \cdots \quad (5.1)$$

The positive coefficients of this expansion for different values of **m** are expressed in terms of triangle of Pascal [76].
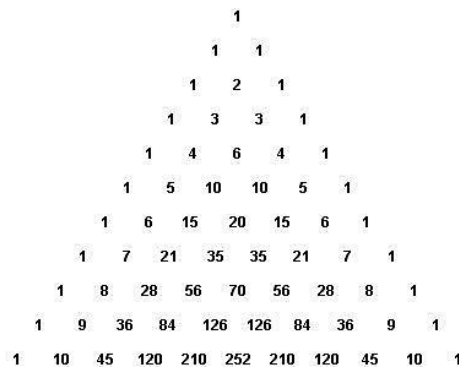
Fig 5.1: Structure of the Triangle of Pascal.

The 'm' illustrates the numbers of components in an array and the coefficients of the expansion illustrate the relative propagations of the components. Usually, this type of array suffers from the practical limitation of bandwidth and efficiency due to the abrupt change in propagation tapering within adjacent components. In this work, the dimensions of the circular

EBGSs are altered proportionally to the relative propagations of the polynomial. We will use the binomial co-efficient for specific EBG numbers and multiply the coefficients with the propagation of the EBG element height for differing the structures.

5.3 Design of LPF Using 1-D Microstrip EBGSs
Design of LPF Using 1-D Microstrip EBGSs is discussing below.

5.3.1. Design Principles

To understand the design of non-uniform distribution, the principle is described by Binomial distribution. As can be seen in the figures, the uniform and the non-uniform circular patterns are engraved with a period '*a*' on the ground surface of standard microstrip T-lines. The important design parameters to achieve a stopband characteristic are the period '*a*' and the filling factor '*r/a*'. Because of the uniform circular pattering EBG, the circles are of the same radius 'r_0' and period '*a*'. For non-uniform pattering EBGSs, the central components have the largest radii of 'r_0' and the radii of the adjacent circles decrease proportionally to the propagation coefficients of the polynomials. Here two relationships within the propagations of the coefficients of the polynomials and the physical dimensions of the EBG circles are proposed. For all the designs the center frequency of the stopband is calculated on an average with the equation of Bragg's condition.
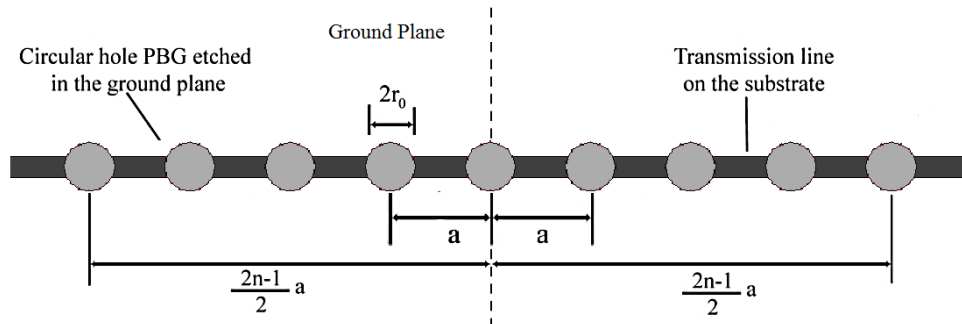
Fig 5.2: Graphical representation of circular uniform EBGS having the radius of r_0 engraved in the ground surface.

For m-element EBG patterns, the nth element's location from the center of the EBG period can be derived from the following equation:

$$d_n = \begin{cases} \dfrac{2n-1}{2}a & \text{for even m} \\ (n-1)a & \text{for odd m} \end{cases} \qquad (5.4)$$

Fig 5.2 and Fig 5.3 show such distribution for even *m*.
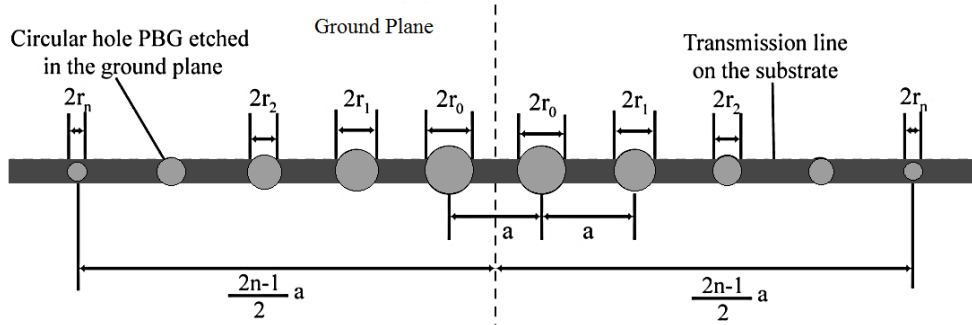
Fig 5.3: Graphical representation of circular non-uniform EBGSs engraved in the ground surface. The central two components have the largest value and the remaining EBGS follow *Chebyshev* distribution.

5.3.2. Non-Uniform EBGSs

Now we discuss some nonuniform EBGSs.

1. Design-1 (Binomial Distribution over circular EBGSs):

The Graphical representation of one lined circular pattering EBGSs using binomial distribution below the 50 Ω T-line is shown in Fig 5.4. The length of the Tx-line is 100 mm and width is 2.263 mm. Here only eight (8) EBG components are engraved in the ground surface. The non-uniform circular pattering EBGSs have the period of 10.44 mm. Because of the radius of non-uniform circular pattering EBGS, we have used the coefficient of the Binomial distribution for 8 component EBGSs. We have wielded Binomial distribution on the radius (r) of each DGS. For N=8 the coefficients are 0.03, 0.2,0.6, 1, 0.6, 0.2, 0.03 and the radius (r) of the EBGSs are taken 0.08, 1.05, 1.57, 2.61, 1.57, 1.05, 0.08mm.
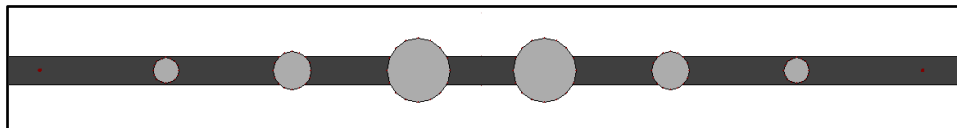
Fig 5.4: Graphical representation of a binomially distributed circular pattering EBGS designed by differing the radius of EBGSs engraved in the ground surface.

2. Design-2 (Binomial Distribution over rectangular EBGSs):

The Graphical representation of one lined rectangular pattering EBGSs using binomial distribution below the 50 Ω T-line is shown in Fig 5.5. The length of the line is 100 mm and width is 2.263 mm. Here also 8 EBG components are engraved in the ground surface and the filing factors are also variable. The non-uniform circular pattering EBGSs have the period of 10.44 mm. Because of the arms of non-uniform rectangular pattering EBGSs, we have used the coefficient of the Binomial distribution for 8 component EBGSs. We have wielded Binomial distribution on the arms of every rectangular pattering EBGS. For N=8 the coefficients are 0.03, 0.2, 0.6, 1, 0.6, 0.2, 0.03 and the arm of the EBGSs are taken 0.08, 1.05, 1.57, 2.61, 1.57, 1.05, 0.08 millimetres.
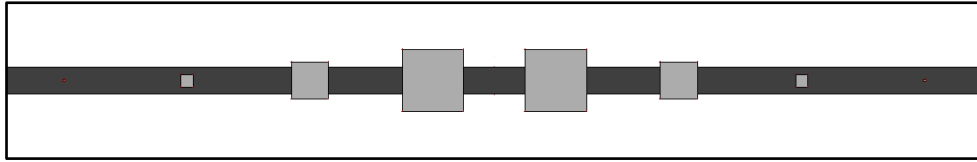
Fig 5.5: Graphical representation of a binomially distributed rectangular pattering EBGS designed by differing the arm lengths of EBGSs engraved in the ground surface.

3. Design-3 (Binomial Distribution over triangular EBGSs):

The Graphical representation of one lined triangular pattering EBGSs using binomial distribution below the 50 Ω T-line is shown in Fig 5.5. The length of the line is 100 mm and width is 2.263 mm. Here also 8 EBG components are engraved in the ground surface and the filing factors are also variable. The non-uniform circular pattering EBGSs have the period of 10.44 mm. Because of the arms of non-uniform triangular pattering EBGSs, we have used the coefficient of the Binomial distribution for 8 component EBGSs. We have wielded Binomial distribution on the arms of every rectangular pattering EBGS. For N=7 the coefficients are 0.03, 0.2, 0.6, 1, 0.6, 0.2, 0.03 and the arm of the EBGSs are taken 0.08, 1.05, 1.57, 2.61, 1.57, 1.05, 0.08 mm.
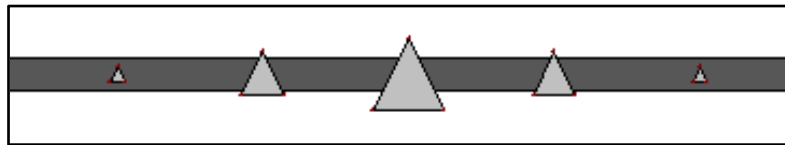
Fig 5.6: Graphical representation of a binomially distributed triangular pattering EBGS designed by differing the arm lengths of EBGSs engraved in the ground surface.

5.3.3. Simulation results of the Non-Uniform EBGSs

The microstrip T-lines to be investigated are: (a) non-uniform EBG components with binomial distributions and (b) non-uniform EBG components with *Chebyshev* distributions. The performances of all the designs are investigated in terms of 10 GHz center frequency under the consideration of negligible ripples in the passband.

1. Design-1 (Binomial Distribution over circular EBGSs):

The S-Parameter performance of EBGSs that is resulted in accordance with the binomial distribution is shown in Fig below.
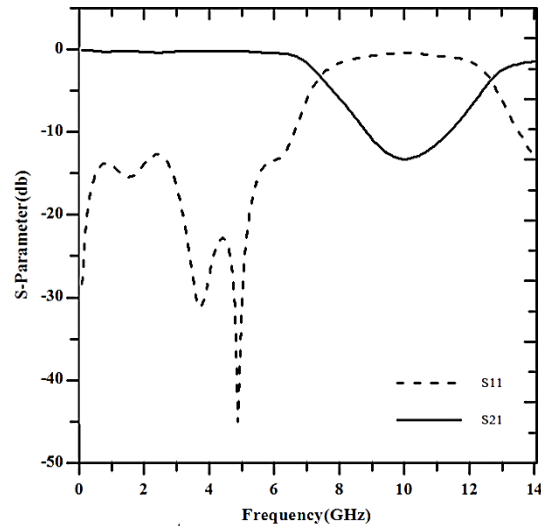
Fig 5.7: S-Parameter performance of a T-line over binomially distributed circular pattering EBGS in accordance with design 1.

It can be seen that the transmission of a signal in the passband is uniformly ensuring minimum ripple height. The 10 dB passband RL BW is found to be 6.88 GHz and the 20 dB rejection bandwidth is not found with maximum isolation of 13.26 dB.

2. Design-2 (Binomial Distribution over rectangular EBGSs):

The S-Parameter performance of EBGSs that is resulted in accordance with the binomial distribution is shown in Fig 5.11.
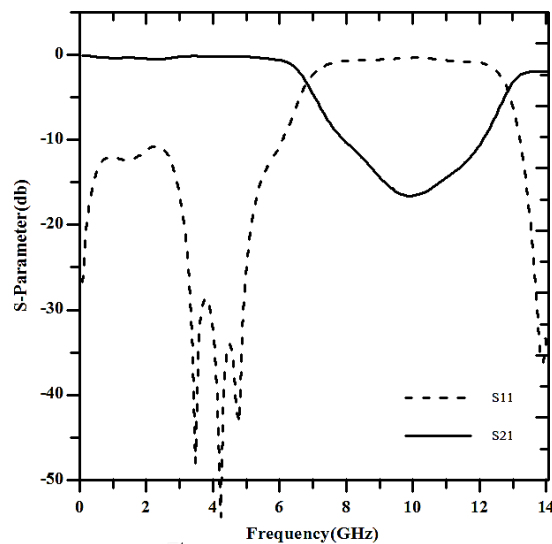
Fig 5.8: S-Parameter performance of a T-line over binomially distributed rectangular pattering EBGS in accordance with design 2.

It can be seen that the transmission of the signal in the passband is uniformly ensuring minimum ripple height. The 10 dB passband RL BW is found to be 7.12 GHz and the 20 dB rejection bandwidth is not found with maximum isolation of 16.59 dB.

3. Design-3 (Binomial Distribution over triangular EBGSs):

The S-Parameter performance of EBGSs that is resulted in accordance with the binomial distribution is shown in Fig 5.12.
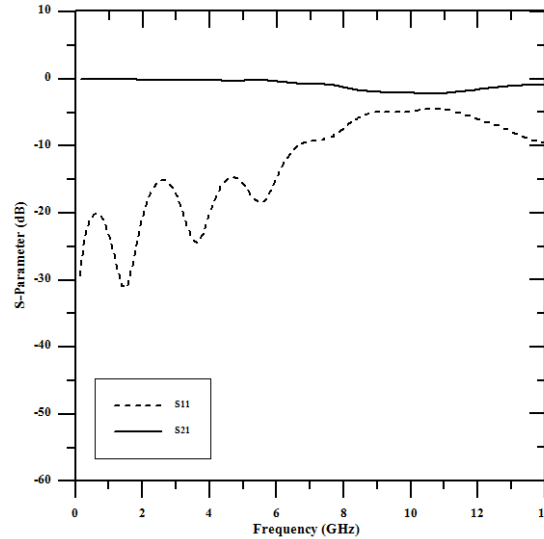
Fig 5.9: S-Parameter performance of a T-line over binomially distributed triangular pattering EBGS in accordance with design 3.

So, from those above three designs and their results describes that this non uniform distribution over conventional EBGS gives smooth passband but if a LPF is needed to establish, it is highly recommended to increase maximum isolation above 20 dB and the rejection bandwidth. So for this reason dumbbell shaped DGS is chosen to fulfill the requirements of the LPFs.

5.3.4. Non-Uniform Triangular Dumbbell-shaped DGSs

The non-uniform EBGSs perform better than the uniform EBGS. So, there is a major chance to find the performance of DGSs with a non-uniform distribution. So, it is necessary to check and simulate some parametric studies of a unit cell of dumbbell shaped DGS so that we could know the performance of it when the designs will be made. The influences of different dimensions of dumbbell-shaped DGS unit cell are presented here. In accordance with the literature here is investigated the parametric studies with some other different values [62].

- **Influence of Dimension of Larger Slot:**

The dimensions of the larger hand of triangular slot had been altered by making b = 180, 200, 220 and 240 mils. The gap and width were maintained constant for all designs having g = 30 mils and w=200 mils. Because of the darker one b=180 mils, Because of the lighter one b=240 mils. The structure of an unit triangular DGS cell is shown in the Fig below.
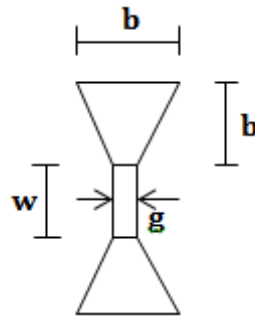
Fig 5.10: A triangular dumbbell shape EBG structure whose length and height is b and gap length is w and gap width is g.

The IL performance of a unit triangular DGS cell is shown in Fig below.
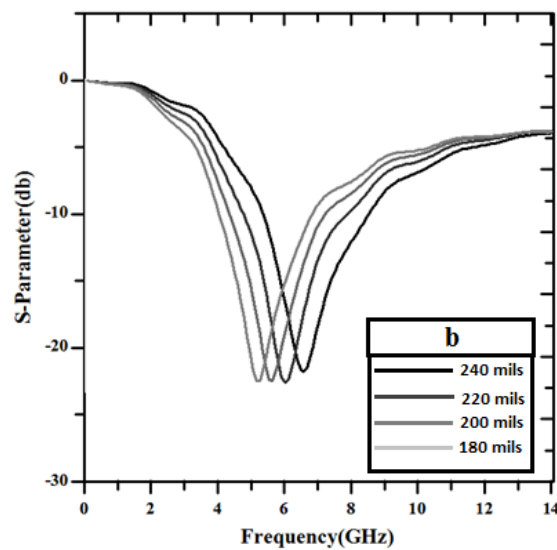
Fig 5.11: IL performance of a unit cell of dumbbell-shaped DGS with variable larger slots of 240, 220, 200 and 180 mils respectively.

From the Fig we can see that, the cut-off frequencies are different for different dimensions. When the dimension is larger, the inductance is increased and the cut-off frequency is decreased. It is also seen that, the attenuation pole locations are also changed.

- **Influence of the Gap Distance of Narrow Slot:**

Gap distances were altered by making g = 20, 30, 40 and 50 mils. The dimension of the larger hand of the triangular slot, b = 104 mils and the width of the narrow slot, w = 50 in all four designs. The IL performance of a unit triangular DGS cell is shown in Fig below.
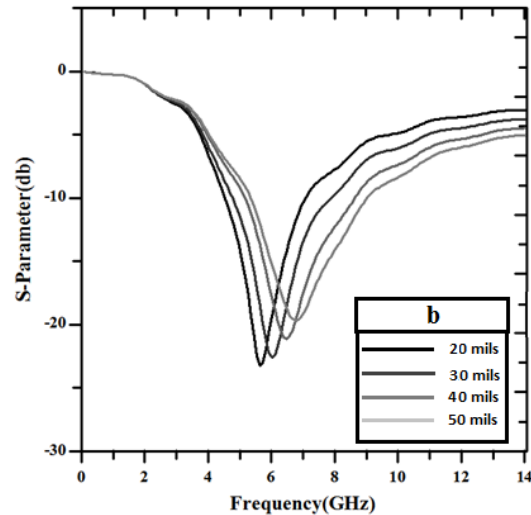
Fig 5.12: IL performance of a unit cell of dumbbell-shaped DGS with variable gap distances of 20, 30, 40 and 50 mils respectively.

It can be seen that the cut-off frequencies are on an average the same. That means the gap distance has no significant influence on the inductance. Rather, it controls the pole location. As the gap distances are increased the gap capacitance decreases and hence the pole location moves up to a higher frequency.

▪ **Influence of width:**

The effect of increasing the width is supposed to provide more capacitance as the increase in the dimension of the slot. On the other hand, the inductive effect will also be significant. It is seen that both the pole location and the cut-off frequencies are influenced by the width of the narrow slot as expected. Increasing width enhances the inductive and capacitive effect. The IL performances with different widths of a unit triangular DGS cell are shown in Fig below.
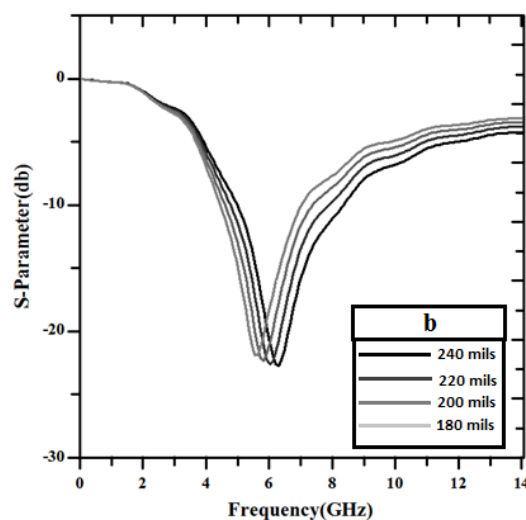
Fig 5.13: IL performance of a unit cell of triangular dumbbell-shaped DGS with the variable width of narrow slots of 240, 220, 200 and 180 mils respectively.

Based on these parametric studies the next investigation will be preceded. The objective is to describe some novel dumbbell-shaped DGSs and hybrid DGSs with the help of the above studies.

❖ **Proposed Triangular Dumbbell-shaped DGSs and Hybrid DGSs**

It is started from a conventional 1-D square pattering periodic dumbbell-shaped DGS structure based on Bragg's condition [60]. The original design is modified to achieve the performance of an LPF. The following designs are investigated.

• **Design-1(Non-Uniform Distribution over larger slot and smaller slot width):**

In design 1, the non-uniform triangular dumbbell-shaped DGS components have the period of 411 mils. The length and width of the largest narrow slot are 50 mils and 200 mils respectively. Because of the length of the larger slot and the gap of the narrow slot of non-uniform dumbbell-shaped DGS, the coefficient of the Binomial distribution for 7 element DGSs have used. Binomial distribution on the length (b) and gap (g) of every DGS has wielded. For N=7 the coefficients are 1, 0.6, 0.2, 0.03. The FF of the central element is 0.5 for both EBGS and narrow slot of the DGS. The design is shown in Fig below.

Fig 5.14: Graphical representation of a binomially distributed LPF designed by differing larger slot width (b) and smaller slot gap (g) of EBGS of dumbbell-shaped DGS engraved in the ground surface.

• **Design-2 (Binomial Distribution over lengths of larger slot with inter leaved uniform circular EBGS):**

In design 2, the width of the larger slot of non-uniform dumbbell-shaped DGS, the coefficient of the Binomial distribution for 7 element triangular DGSs and inter-leaved uniform circular EBGS have used. Binomial distribution on the length (b) of every DGS has wielded. For N=7 the coefficients are 1, 0.6, 0.2, 0.03 and the length (b) of the EBGSs are taken 200, 120, 40, 6 mils. The FF of the central element is 0.5. The design is shown in Fig below.

Fig 5.15: Graphical representation of a binomially distributed LPF designed by differing larger slot width (b) of EBGS of triangular dumbbell-shaped DGS and inter-leaved EBGSs engraved in the ground surface.

- **Design-3(Binomial Distribution over lengths of larger slot inter-leaved non-uniform circular EBGS):**

In design 3, the width of the larger slot of non-uniform dumbbell-shaped DGS, the coefficient of the Binomial distribution for 7 element triangular DGSs and inter-leaved binomially distributed circular EBGS have used. Binomial distribution on the length (b) of every DGS has wielded. For N=7 the coefficients are 1, 0.6, 0.2, 0.03 and the length (b) of the EBGSs are taken 200, 120, 40, 6 mils. The FF of the central element is 0.5. The design is shown in Fig below.

Fig 5.16: Graphical representation of a binomially distributed LPF designed by differing larger slot width (b) of EBGS of triangular dumbbell-shaped DGS and inter-leaved EBGSs engraved in the ground surface.

- **Design-4(Binomial Distribution over lengths of larger slot inter-leaved uniform triangular EBGS):**

In design 4, Taconic substrate having dielectric constant 2.45 and height of 31 mils have used. Because of the width of the larger slot of non-uniform dumbbell-shaped DGS, the coefficient of the Binomial distribution for 7 element triangular DGSs and inter-leaved uniform triangular EBGS have used. Binomial distribution on the length (b) of every DGS has wielded. For N=7 the coefficients are 1, 0.6, 0.2, 0.03 and the length (b) of the EBGSs are taken 200, 120, 40, 6 mils. The FF of the central element is 0.5. The design is shown in Fig 5.23.
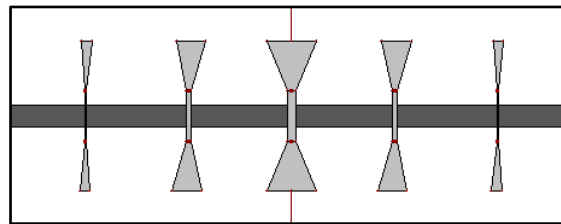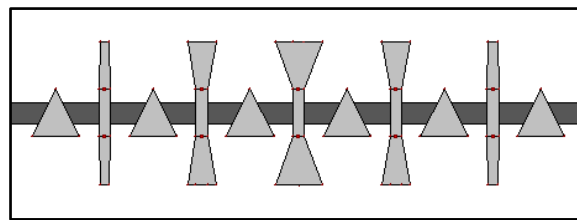

Fig 5.17: Graphical representation of a binomially distributed LPF designed by differing larger slot width (b) of EBGS of triangular dumbbell-shaped DGS and inter-leaved EBGSs engraved in the ground surface.

- **Design-5(Binomial Distribution over lengths of larger slot inter-leaved non-uniform rectangular EBGS):**

In design 5, the width of the larger slot of non-uniform dumbbell-shaped DGS, the coefficient of the Binomial distribution for 7 element triangular DGSs and inter-leaved binomially distributed rectangular EBGS have used. Binomial distribution on the length (b) of every

DGS and width of rectangular EBGS has wielded. For N=7 the coefficients are 1, 0.6, 0.2, 0.03 and the length (b) of the EBGSs are taken 200, 120, 40, 6 mils. The FF of the central element is 0.5. The design is shown in Fig below.
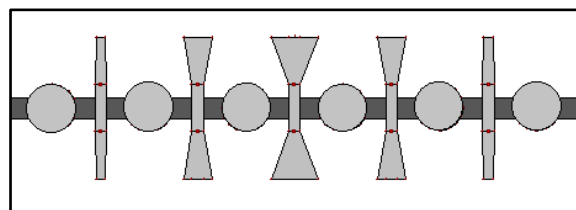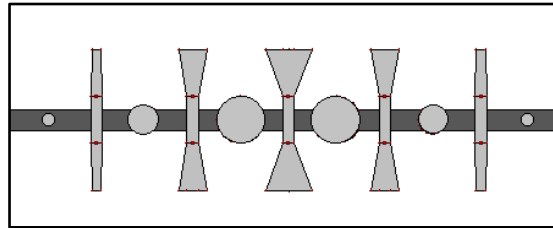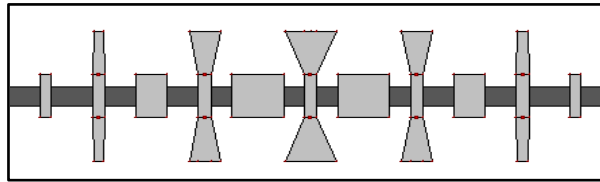

Fig 5.18: Graphical representation of a binomially distributed LPF designed by differing larger slot width (b) of EBGS of triangular dumbbell-shaped DGS and length of inter-leaved EBGSs engraved in the ground surface.

5.3.5. Performances of Triangular Dumbbell-shaped DGSs

S-Parameter performances of different novel designs have been investigated. The taconic substrate with dielectric constant of 2.45 and thickness of 31 mils are used in all designs. The RL and IL performances have been investigated.

- **Design-1:**

The S-Parameters vs. frequency of Design 1 is shown in Fig below. It can be seen that the passband ripples are of 2 dB near cut-off. Maximum isolation of the rejection band is -55 dB and minimum isolation is -19 dB. The cut-off frequency is about 4 GHz. But it is observed that the RL curve is almost straight after 4GHz. Average 10 dB RL-BW is 4.4 GHz, 3 dB cut-off frequency is 4.2 GHz, 20 dB IL-BW is 17.5 GHz and maximum peak of IL is -55 dB.

Fig 5.19: S-Parameter performance of a T-line over DGSs in accordance with design 1.

- **Design-2:**

The S-Parameters vs. frequency of a dumbbell shape DGS with interleaved EBGS of Design 2 is shown in Fig below. Frequency shifting is found to be 1.25% at -3dB point in the IL curve. It has also observed that the RL curve is almost straight after 4.8 GHz. Maximum isolation of the rejection band is -68 dB and minimum isolation is -25 dB. Average 10 dB RL-BW is 4.8 GHz, 3 dB cut-off frequency is 4.8 GHz, 20 dB IL-BW is more than 19 GHz and maximum peak of IL is -68 dB.
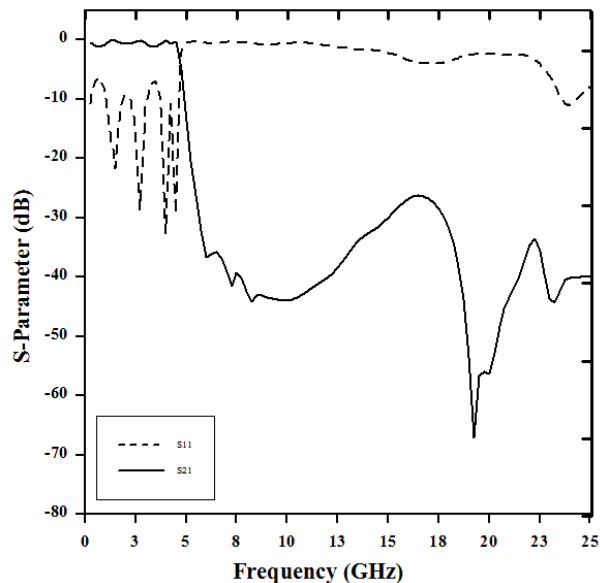
Fig 5.20: S-Parameter performance of a T-line over hybrid dumbbell-shaped DGSs in accordance with design 2.

- **Design-3:**

The S-Parameters vs. frequency of a dumbbell shape DGS with interleaved EBGS of Design 3 is shown in Fig below. Maximum isolation of the rejection band is -53 dB and minimum isolation is -17 dB. The passband of the IL curve is smoother and the rejection band curves are below -20dB and going down gradually. The changing of the width of EBGS of dumbbell-shaped DGS and at the same time the changing of the length of interleaving EBGSs has caused a great impact on the results. Average 10 dB RL-BW is 4.1 GHz, 3 dB cut-off frequency is 4.8 GHz, 20 dB IL-BW is 9 GHz and maximum peak of IL is -53 dB.
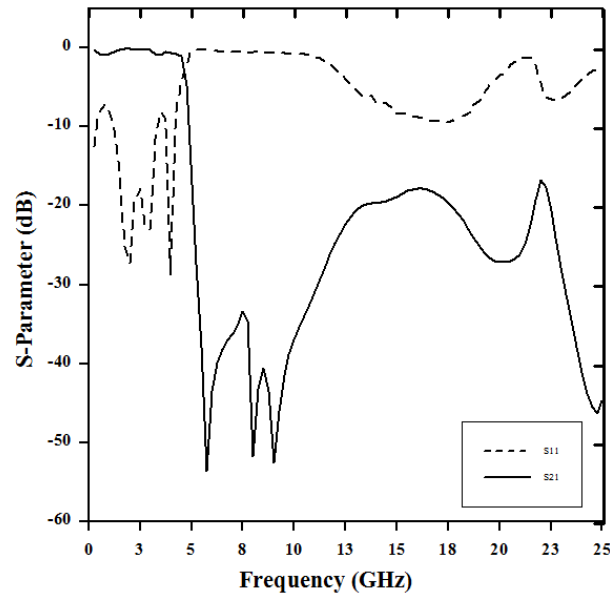
Fig 5.21: S-Parameter performance of a T-line over hybrid dumbbell-shaped DGSs in accordance with design 3.

- **Design-4:**

The S-Parameters vs. frequency of Design 4 is shown in Fig below. It can be seen that the RL curve is almost straight after 4GHz. Maximum isolation of the rejection band is -53 dB and minimum isolation is -19 dB. Average 10 dB RL-BW is 4.1 GHz, 3 dB cut-off frequency is 4.4 GHz, 20 dB IL-BW is 16.5 GHz and maximum peak of IL is -53 dB.
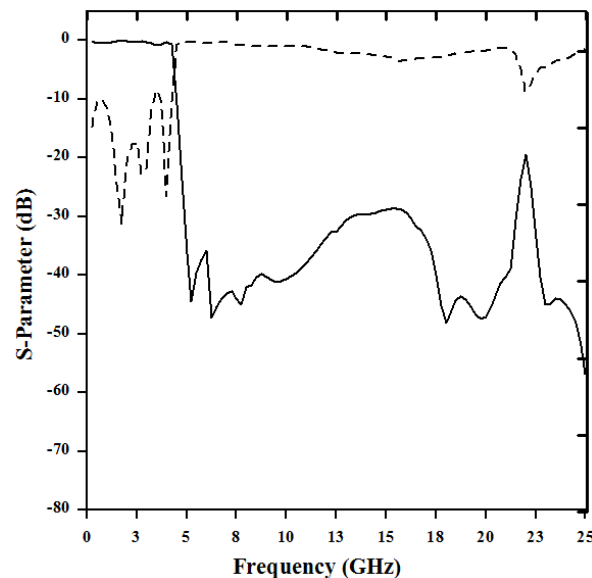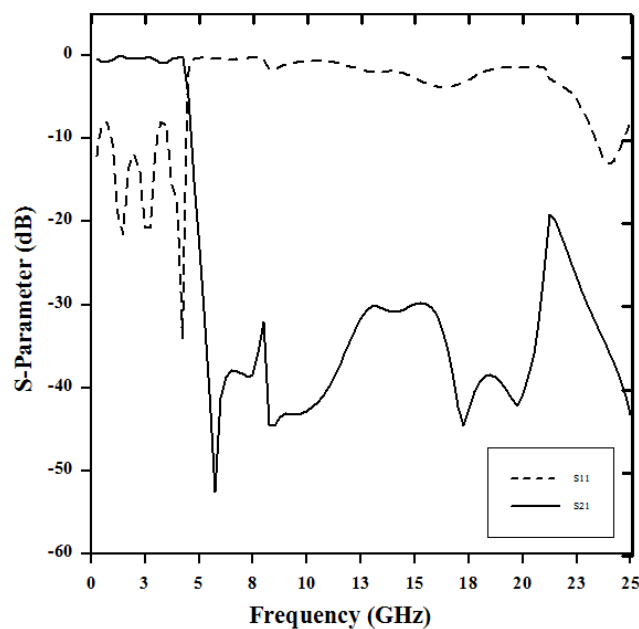

Fig 5.22: S-Parameter performance of a T-line over dumbbell-shaped DGSs in accordance with design 4.

- **Design-5:**

The S-Parameters vs. frequency of Design 5 is shown in Fig below. Frequency shifting is found to be 2.5% at -3dB point in the IL curve. After 4.5 GHz the slope of the IL curve has gone down sharply. It has also observed that the RL curve is almost straight after 5 GHz. It is observed that there is some ripple on the passband in the IL curve. There is an observable ripple about -2dB. Maximum isolation of the rejection band is -55 dB and minimum isolation is -23 dB. Average 10 dB RL-BW is 3.6 GHz, 3 dB cut-off frequency is 4.4 GHz, 20 dB IL-BW is more than 19 GHz and maximum peak of IL is -55 dB.
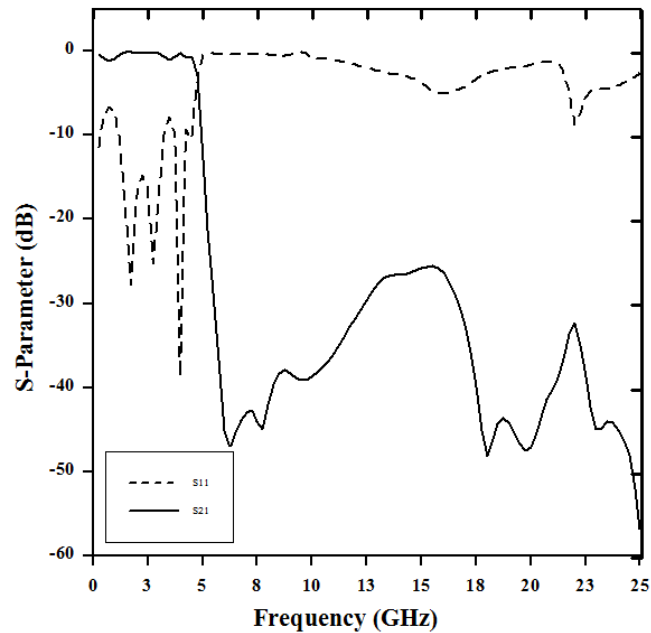
Fig 5.23: S-Parameter performance of a T-line over hybrid DGSs in accordance with design 5. The substrate is Taconic with dielectric constant= 2.45 and height= 31 mils.

Table 5.1: Presentation of the designs with their S-Parameter performances.
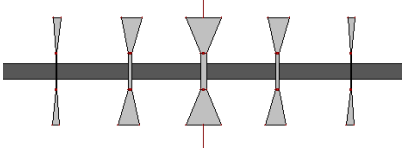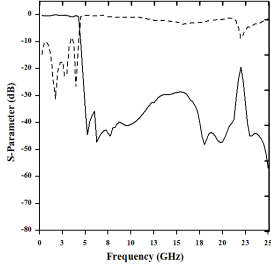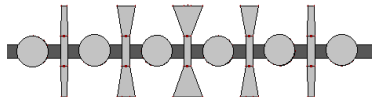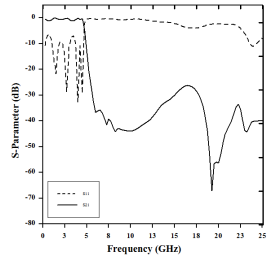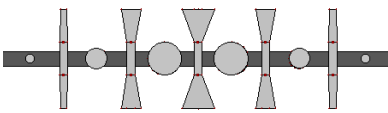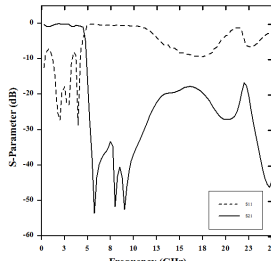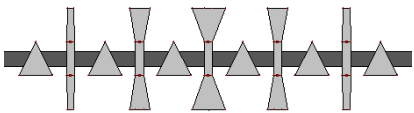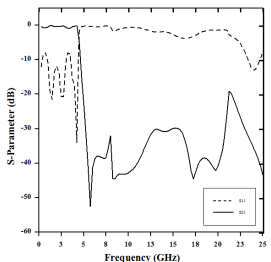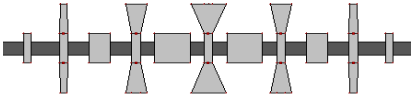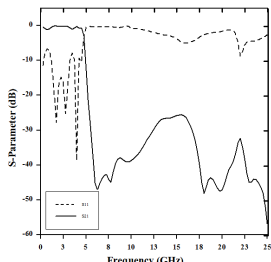
No	Designs	S-Parameter Performance
1.		
2.		
3.		
4.		
5.		

Table 5.2: Comparison of S-Parameter performances of the designs.

Design No	10 dB RL-BW	3 dB cutoff frequency	20dB IL-BW	Maximum Peak of IL
1.	4.4 GHz	4.2 GHz	17.5 GHz	-55 dB
2.	4.8 GHz	4.8 GHz	>19 GHz	-68 dB.
3.	4.1 GHz	4.8 GHz	9 GHz	-53 dB
4.	4.1 GHz	4.4 GHz	16.5 GHz	-53 dB
5.	3.6 GHz	4.4 GHz	>19 GHz	-55 dB

From the data of table we can conclude that design 2 and design 5 gives the best performance because of the IL bandwidth. But in design 5 is better from design 2 Because of the sharpness of the passband.

5.4. Validification of the simulation result

- **T-line IL result**

The characteristic of an ideal T-line is that if the signal enters into the ideal T-line, the output we get is exactly the same as the input signal. From the Fig of IL performance of the T-line, it is clear that our simulation is validated.
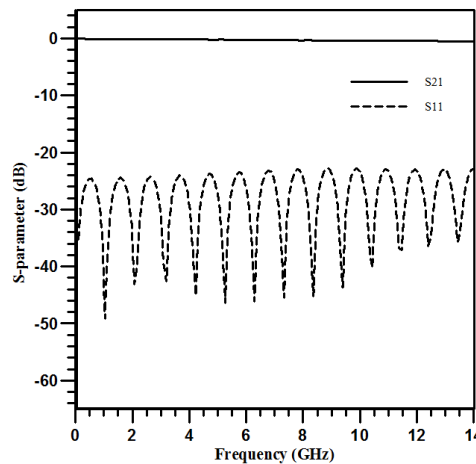
Fig 5.24: S-Parameter performance of an ideal 50Ω T-line.

- **Reason for substituting 1-D designs from 2-D designs**

From the investigation, we have seen that 1-D and 2-D designs both give almost the similar performance. So we choose 1-D designs Because of the miniaturization or compactness of designs. The S-Parameter performances of 2-D and 1-D circular shaped EBGSs are given below.
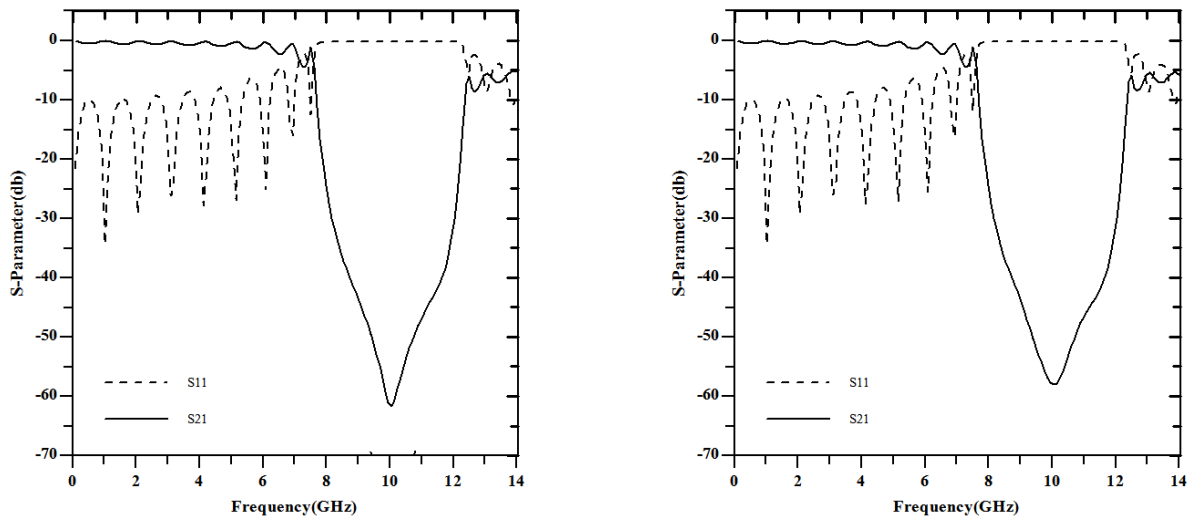
Fig 5.25: Simulated S-Parameter performances of a standard 50 Ω T-line perturbed by 2-D (three lines) (left) and 1-D (one line) (right) uniform circular EBGSs in the ground surface.

5.5.   Validation of the measured result with software design result.

For validating our software result, the one of the measured result [71] has been chosen and with the same design we have simulated our output and compare both results. One of the designs form the journal which has the measured result is redrawn by Zeland IE3D below.
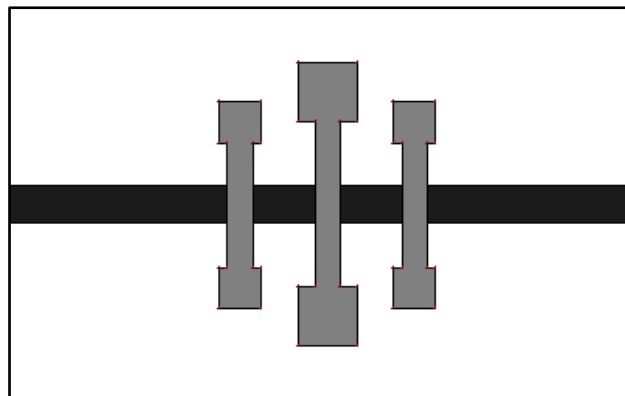
Fig 5.26: Design configuration for LPF with fabricated design in accordance with research paper [71].

In figure a microstrip LPF is shown. This LPF is also designed using 50 Ω, $\lambda_g/4$ microstrip line. In this design configuration the specifications are dielectric constant (ε) = 3.38, height of substrate (h) = 1.524 mm, thickness of conductor (t) = 0.07 mm and loss tangent (tanδ) = 0.0025. The design goals for designing this LPF are 3-dB cutoff frequency = 6.6 GHz, IL in passband 0.5-dB, 20-dB attenuation from 7.4 GHz to 10 GHz. The geometry generated by Zeland IE3D and measuring result is shown together in figure.
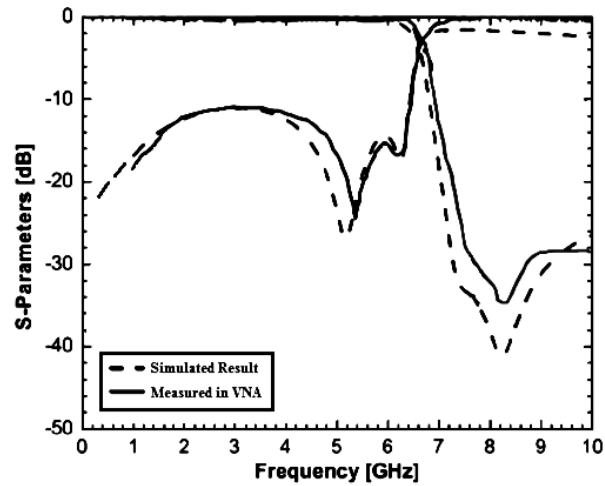
Fig 5.27: Simulation result compared with measured result of S-Parameter performances of LPF with dumbbell shaped DGS.

From the results of above figure it can clearly conclude that the measured result is identical to our software simulation result. This proves the validification of the software simulation.

5.6. Physical representation of some designs

Table 5.3: Representation of some structures with their physical structures according to their designs.

Design no	Graphical Representation	Physical Representation
1		
2		
3		
4		
T-line		

5.7. Summary

So, the total summary in this chapter is the frequency properties of the unit cell of a triangular dumbbell-shaped DGS and the whole structures based upon the properties have been investigated. In dumbbell-shaped DGS the dimension of larger slots controls the cut-off frequencies. Another set of regular EBGSs has been inserted in within the inter cell distance of dumbbell-shaped DGSs. At first, few structures are investigated to yield better LPF performance in terms of passband RL BW, ripple-free transmission and wider stopband. The graphical result of design 3 and design 4 gives the sharper slope of passband properties and ripples are less. But IL bandwidth is greater in design 4. So design 4 is much better than design 3. The modified triangular dumbbell-shaped DGS and hybrid DGS show the wider stopband and the smoother passband as of the LPF properties.

Chapter-6

Conclusions

6.1 Summary of Project Contributions

Defective ground structures are the well-known microwave components in recent years for its reduced size or structures. These component features are very attractive in microwave engineering. They used in low temperature co-fired ceramics and ferrites, substrate integrated waveguides, metamaterials or complementary split-ring resonators. Defective structures are recently been used for improving the performance of microwave circuits/ components. Some factors depend on the altitude and width of the stopband. FFs, periods, number of components and substrate properties are most common factors. The uniform conventional circular, square pattering EBGSs and the dumbbell-shaped DGS have been investigated. One line and three line EBGS have been analyzed, Different conditions on this EBGSs are investigated for our main project purpose. From the results we have been concluded that one line, non uniform binomial distribution and seven to ten elements have been considered for progressing our project.

In chapter 4, we have investigated the three lines and one line circular, rectangular and triangular EBGS engraved on the ground surface. Then, we had concluded that one line gives the similar performance as three lines EBGSs. Then we had investigated same area of uniform EBGSs. Then, we had investigated by increasing the filling factor and increasing the number of EBGSs. Then, the uniform dumbbell shaped DGS engraved in the ground surface and the compactness is investigated.

In chapter 5, firstly, conventional non-uniform EBGSs have been investigated. Next, a unit triangular dumbbell shaped DGS characteristics have been investigated. Finally, the triangular shaped DGSs and hybrid DGSs have been proposed and investigated.

After completing all the research work we can decide our conclusion that non uniform binomially distributed deigns provide much better results than our conventional works as discussed in our literatures. For squared pattering DGSs the FFs can be considered as 0.5 and used in two larger slots of DGS. We can be considered the range of 0.4 to 0.5 as our optimized FF. Recent works and this project works convey the frequency dependence of this performance. We also conclude the common factor is the frequency shifting and the center frequencies are totally dependent on the designs and Bragg's condition controls it. Our another goal is to perform the shifting to less than the conventional and we achieved the 200% reduced performance from our design. Last of all, the simulations have been performed on the infinite ground surface.

6.2 Recommendation For Future Works

This project work has been completed by commercial EM software Zeland IE3D. The project has many future works. The researchers could be research on theoretical modeling. Though it is a complex geometry and it is hard to calculate the propagation constant, the future job could be the reduction of complexity of this geometry. The future works could be on different designs like dual T-line, U or W shape geometry. There is another scope for this project that is the researching proper algorithms and mathematical calculations for the proper design like the conventional methods (insertion loss or image parameter methods). Now there is no perfect method of analyzing exact parameters or sizes of DGSs or EBGSs for the design of filters and for the particular performance where the perfect EBGSs can be chosen. Though VNA can measure the S-Parameter performances of the EBGSs so the future analyzes need to be justified experimentally and compared with simulated results by this device.

References

[1]   Li Yang, M.Fan, F.Chen, J.She, Z.Feng, "A Novel Compact Electromagnetic Bandgap (EBG)StructureandItsApplicationsforMicrowaveCircuits",*IEEETrans.Microw.Theory Techn.*, Vol. 53, No.1, pp. 183-190,Jan. 2005.

[2]   J.Liang, H.Y.D.Yang,"Microstrip Patch Antennason Tunable Electromagnetic Band-Gap Substrates," *IEEE Trans. On Microw. Theory Tech.,* Vol. 57, pp. 1612-1617, No.6, Jun. 2009.

[3]   P. Baccarelli, et al., "Dispersive Analysis of Wide-Bandstop Compact EBG Microstrip Lines for Filter Applications", International Symposium on Microwave and Optical Technology, Rome, Italy, 2007.

[4]   R.S. Kshetrimayum, L. Zhu, " EBG Design using FSS Elements in Rectangular Waveguide", *Appl. Comp. Electrom. Society*, Vol. 21, NO. 2, Mar. 2006.

[5]   R.Verma, K. Daya, "Effect of Forbidden Bands of Electromagnetic Bandgap Engineered Ground Plane on the Response of Half Wave Length Linear Microwave Resonator", *J. Appl. Phys*vol. 109, no. 8, pp. 084505, Apr. 2011.

[6]   E. Yablonovitch, "Inhibited spontaneous emission in solid-state physics and electronics", *Phys. Rev. Lett.*, vol. 58, pp. 2059-2063, 1987.

[7]   S. John, "Strong Localization of Photons in Certain Disordered Dielectric Super Lattices ," *Phys. Rev. Lett*. 58, 2486, 1987.

[8]   Md. S. Alam, N. Misran, B. Yatim, and Md. T. Islam, "Development of Electromagnetic Band Gap Structures in the Perspective of Microstrip Antenna Design", *Int. J. Antennas and Propagation*, vol. 2013, pp. 22, 2013.

[9]   P. de Maagt, R. Gonzalo, Y. C. Vardaxoglou, and J. M. Baracco, "Electromagnetic bandgap antennas and components for microwave and (sub)millimeter wave applications ," *IEEE Trans. Antennas and Propagation*, vol. 51, no. 10 , pp. 2667–2677, 2003.

[10]   M. S. Alam, et al., "Design analysis of an electromagnetic bandgap microstrip antenna," *The American Journal of Applied Sciences*, vol. 8, no. 12, pp. 1374–1377, 2011.

[11]   D. Sievenpiper, "Review of theory, fabrication, and applications of high impedance ground planes," in Metamaterials: Physics and Engineering Explorations, N. Engheta an d R. Ziolkowski, Eds., chapter 11, John Wiley & Sons, New York, NY, USA, 2006.

[12]   G. H. Li, X. H. Jiang, and X. M. Zhong, "A novel defected ground structure and its application to a lowpass filter," *Microw. Optic. Tech.Lett.*, vol. 48, no. 9, pp. 1760–1763, 2006.

[13]   C. S. Kim, et al., "Equivalent circuit modelling of spiral defected ground structure for microstrip line," *Electro.Lett.*, vol. 38, no. 19, pp. 1109–1110, 2002.

[14]   M. Islam and M. Alam, "Design of high impedance electromagnetic surfaces for mutual coupling reduction in patch antenna array," *Materials*, vol. 6, pp. 143–155, Jan. 2013.

[15]   M. Faruque, M. Islam, and N. Misran, "Evaluation of specific absorption rate (SAR) reduction for PIFA antenna using metamaterials," *Frequenz*, vol. 64, no. 7-8, pp. 144–149, 2010.

[16]   M. Faruque, M. Islam, and N. Misran, "Study of specific absorption rate (SAR) in the human head by metamaterial attachment," *IEICE Electronics Express*, vol. 7, no. 4, pp. 240–246, 2010.

[17]   M. Islam, M. Faruque, and N. Misran, "SAR reduction in a muscle cube with metamater ial attachment," *Applied Physics*, vol. 103, no. 2, pp. 367–372, 2011.

[18]   T. Lopetegi, M. Laso, R. Gonzalo et al., "Electromagnetic crystals in microstrip technology," *Optical and Quantum Electronics*, vol. 34, no. 1–3, pp. 279–295, 2002. ·

[19]   F. Yang, K. Ma, M. Qian, and T. Itoh, "A uniplanar compact photonic-bandgap   (UC-PBG) structure and its applications for microwave circuits," *IEEE Trans. Microw. Theor y Tech*, vol. 47, no. 8, pp. 1509–1514, 1999.

[20]   M. Mollah, N. Karmakar and J. Fu, 'Uniform circular photonic bandgap structures (PBGSs) for harmonic suppression of a bandpass filter', *AEU - International Journal of Electronics and Communications*, vol. 62, no. 10, pp. 717-724, 2008.

[21]   N. Karmakar, M. Mollah, S.Padhi and R. Lim Li Ling, "Investigations into Planar Electromagnetic Bandgap," *IEEE Trans. Microw. Theory Tech.,* vol 25, no 5, pp. 419-426, Dec. 2006.

[22]   M. Mollah, N. Karmakar and J. Fu, 'Investigation of novel tapered hybrid defected ground structure (DGS)', *Int. J RF and Microw. Comp. Aid. Eng.*, vol. 15, no. 6, pp. 544-550, 2005.

[23]   Chul-Soo Kim, Jun-Seok Park, Dal Ahn and Jae-Bong Lim, 'A novel 1-D periodic defected ground structure for planar circuits', *IEEE Microw. Guid. Wave Lett.*, vol. 10, n o. 4, pp. 131-133, Apr. 2000.

[24]   T. Euler, J. Papapolymerou, "Silicon Micromachined EBG Resonator and Two-Pole Filter with Improved Performance Characteristics," *IEEE Microw. Wirel.Compon. Lett*, vol. 13 no. 9,pp. 373,2003.

[25]   Hsiuan-ju Hsu, M. Hill, R. Ziolkowski and J. Papapolymerou, 'A Duroid-based planar EBG cavity resonator filter with improved quality factor', *Antennas Wirel. Propag. Lett.*, vol. 1, no. 1, pp. 67-70, 2002..

[26]   W. J. Chappell, M. P. Little, and L. P. B. Katehi, "High Isolation, Planar Filters Using EBG Substrates," *IEEE Microw. Wirel.Compon. Lett*., vol. 11, No. 6, pp. 246-248,2001.

[27]   W. Chappell and Xun Gong, "Wide bandgap composite EBG substrates", *IEEE Trans. Antennas Propagat.*, vol. 51, no. 10, pp. 2744-2750, 2003.

[28]   J. Vardaxoglou, "Tunable Metallodielectric Electromagnetic Band Gap (MEBG) Structures with defects", in *IEEE International Conference on Electromagnetics in Advanced Applications*, Torino, Italy, 2003, pp. 667-670.

[29]   M. Hill, R. Ziolkowski, amd J. Papapolymerou, "A High-Reconfigurable Planar EBG Cavity Resonator*," IEEE Microw. Wirel. Comp.Lett.*, vol. 11, No. 6, pp. 255-257, 2001.

[30]   V. Radisic, Y. Qian, R. Coccioli, and T. Itoh, "Novel 2-D photonic bandgap structures for microstrip lines," *IEEE Microw.Guid. Wave Lett.,*vol. 8 no. 2, pp. 69-71, Feb. 1998.

[31]   T. Lopetegi, M. Laso, J. Hernandez, M. Bacaicoa, D. Benito, M. J. Garde, M. Sorolla, and M. Guglielmi, "New Microstrip Wiggly - Line Filters with Spurious Passband Suppression," *IEEE Trans.Microw. Theory Tech*., vol. 49, no. 9, pp. 1593-1598, 2001.

[32]   D. Nesic, "A New Type of Slow-Wave 1-D PBG Microstrip Structure without Etching in the Ground Plane for Filter and Other Applications," *Microw. Optic. Tech. Lett*., Vol. 33, No. 6, pp. 440-443, 2002.

[33]   D. Nesic, "A New Type of Slow-Wave 1D PBG Microstrip Band-Pass Filter," *Microw. Optic. Tech. Lett*., Vol.37, No.3, pp.201-203,2003.

[34]   D. M. Pozar*, Microwave Engineering*. Reading, MA: Addison-Wesley, 1990.

[35]   V. Radisic, Y. Qian, and T. Itoh, "Novel architectures for high-efficiency amplifiers for wireless applications," *IEEE Trans. Microw. Theory Tech*. vol.46. no. 11, pp. 1901-1909, Nov. 1998.

[36]   M. Rahman and M. Stuchly, "Transmission line – periodic circuit representation of planar microwave photonic bandgap structures,"*Microw. Optic. Tech. Lett*., vol. 30, no. 1,pp. 15–19, 2001.

[37]   Paul J. Schields, "Bragg's Law and Diffraction," Center for High Pressure Research, State University of New York, Stony Brook, NY 11794-2100. http://www.eserc.stonybrook.edu/ProjectJava/Bragg/

[38]   C. Balanis, *Antenna theory*. Hoboken, NJ: Wiley Interscience, 2005.

[39]   M. Mollah, "Planar Electromagnetic Bandgap Structures and Applications", Ph.D, Nanyang Technological University, Singapore, Mar. 2005.

[40]   Y. Sung., "Tunable BandStop Filter Based Defected Ground Structure using a Metal Plate", *Microw. Optic.Tecn.Lett*., Vol. 51, No. 9, pp. 2254-2255, 2009.

[41]   M.Laso, T. Lapetegi, M. Erro, D. Benito, M. J. Garde and M. Sorolla, "Multiple-Frequency-Tuned Photonic BandgapMicrostrip Structures", *IEEE Microw.Guid.Wave Lett.*, vol. 10, No. 6, pp. 220-222, 2000.

[42]   S. Tse, B. SanzIzquierdo, J.Batchelor and R. Langley, "Reduced sized Cells for Electromagnetic Bandgap Structures," *Electron. Lett*., vol. 39, No. 24, pp. 1699, 2003.

[43]   G. Goussetis, A.Feresidis and J. Vardaxoglou, "Periodically loaded 1-D metallo dielectric electromagnetic bandgap structures for miniaturisation and bandwidth enhancement", *IEE Proceedings - Microwaves, Antennas and Propagation*, vol. 151, no. 6, p. 481, 2004..

[44]   A. Feresidis, G. Apostolopoulos, N. Serfas and J. Vardaxoglou, "Closely Coupled Metall odielectric Electromagnetic Band-Gap Structures Formed by Double-Layer Dipole

and Tripole Arrays", *IEEE Trans. Antennas Propagat.*, vol. 52, no. 5, pp. 1149-1158, 2004.

[45] J. Vardaxoglou, G. Gousetis and A. Feresidis, "Miniaturisation schemes for metallodielectric electromagnetic bandgap structures", *IET Microw. Antennas Propag.*, vol. 1, no. 1, p. 234, 2007.

[46] G. Goussetis, A. Feresidis and J.Vardaxoglou,"Performance of Metallodielectric EBG Structures with Periodic Loaded Elements", in *IEE Seminar on Metamaterials, for Microwave and (Sub)Millimetre Wave Applications*, London, UK, 2003.

[47] S. M. Shakil Hassan, Md. Nurunnabi Mollah, "Offset EBGS against tapered EBGS: Substantial reduction of microstrip stopband filter in size", in IEEE Region 10 Conference (TENCON), Singapore, 2016.

[48] S. M. Shakil Hassan, Nurunnabi Mollah, Khandkar Raihan Hossain, "Observation of low-pass performance from novel trapezoidal slotted dumbbell shape EBGS", 2nd International Conference on Electrical Information and Communication Technologies (EICT), Khulna, Bangladesh, 2016.

[49] A. Feresidis, A. Chauraya, G.Goussetis, J. Vardaxoglou and P. deMaagt, "Multiband Artificial Magnetic Conductor Surfaces", in *IEE Seminar on Metamaterials forMicrowave and (Sub) Millimetre Wave Applications*, London, UK, 2003.

[50] S. Haykin, *Communication Systems*, Third Edition, New York, Wiley,1994.

[51] David M. Pozar, *Microwave Filters*, Fourth Edition, New Jersey, Wiley,1998.

[52] Wikipedia, 'Filter (signal processing)', 2015. [Online]. Available: http://en.wikipedia.org/wiki/Filter_ (signal_processing).

[53] J. Shumpert, T. Ellis, G. Rebeiz and L. Katehi, "Microwave and Millimeter-Wave Propagation in Photonic Band-Gap Structures," AP-S/URSI, pp. 678, Oct. 1997.

[54] C. Soukoulis, "The History and Review of the Modelling and Fabrication of Photonic Crystals", *Nanotechnology*, vol 13,pp 420-423, 2002

[55] D. Prather, S. Shi, A.Sharkawy, J. Murakowski and G.J. Schneider,"*Photonic Crystals: Theory, Applications, and Fabrication*", N. J,Wiley 2009.

[56] F. Falcone, T. Lopetegi, M. Sorolla, "1D and 2D Photonic BandGapMicrostrip Structures," *Microw. Optic. Techn. Lett*, Vol. 22, No. 6, 1999.

[57] G. Cakir, L. Sevgi, "Design of A Novel Microstrip Electromagnetic BandGap (EBG) Structures," *Microw. Optic.Techn.Lett.*, Vol. 46, No. 4, pp 399-401, 2005.

[58] J. D. Joannopoulos, R. D. Meade and J. N. Winn, "Photonic Crystals: Molding the Flow of Light", New Jersey: Princeton University Press, 1995.

[59] M. Laso, M. Erro, D. Benito, M. Grade, T. Lapetegi, F. Faleone, and M. Sorolla, "Analysis and Design of 1D Photonic BandGapMicrostrip Structure using a Fiber Grating Model", *Microw. Optic.Tech.Lett.*, vol. 22, No. 4,pp 223-226, 1999.

[60] T. Akaline, M. A. G. Laso, T. Lopetgi, and O. Vanbesien, "PBG-type microstrip filters with one-end and two-sided patterns," *Microw. Optic. Tech. Lett.*, vol. 30, no. 1,pp 69-72, Jul. 2001.

[61] D. Nesic and A. Nesic, "Bandstopmicrostrip PBG filter with sinusoidal variation of the characteristic impedance and without etching in the ground plane," *Microw. Optic. Tech. Lett.*, vol. 29, no. 6, pp. 418-420, Jun. 2001.

[62] Q. Xue, K. M. Shum and C.H Chan, "Novel 1-D photonic bandgap microstrip transmission line," APS-International symposium, 2000, IEEE, vol. 1, page(s), 354-356.

[63] Y. Qian, R. Coccioli, F-R. Yang and T. Itoh "Passive and active component design using PBG," Terahertz Electronics proceedings, 1998, IEEE sixth Int. Conf., pp. 42-45.

[64] H. W. Liu, Z. F. Li, and X. W. Sun, "A novel fractal defected ground structure and its a pplication to the low-pass filter," *Microwave ant Opt. Tech. Lett.* vol. 39, no. 6 pp. 453-456, Dec. 2003.

[65] Y. Qian, F.R. Yang, and T. Itoh, "Characteristics of microstrip lines on a uniplanar compact PBG ground plane," *1998 Asia-Pacific Microwave Conf. Dig.,* pp.589-592, Dec. 1998.

[66] J. Bahl and P. Bhartia, *Micorwave solid state circuit design*, Wiley, New York, 1998.

[67] G. Larkins, R. Socorregut and Y. Vlasov, 'Superconducting microstrip hairpin filter with BaTiO/sub 3/ patches', *IEEE Trans. Appl. Supercond.*, vol. 13, no. 2, pp. 724-726, Jun. 2003.

[68] DušanNešić, "A brief Review of Microwave Photonic Bandgap (PBG) Structures", Mikrotalasnarevija, vol. 7, iss. 1, pp. 18-24, 2001

[69] R. Levy, R. Snyder and G. Matthaei, "Design of microwave filters," IEEE Transactions on Microwave Theory & Techniques, Vol. 50, No. 3, pp. 783-793, Mar. 2002.

[70] P. I. Richards, "Resistor-Transmission Line Circuits," *Proceedings of the IRE*, vol. 36, pp. 217–220, Feb. 1948.

[71] Arjun Kumar, M.V. Kartikeyan, " Design and realization of microstrip filters with new d efected ground structure (DGS)," *Eng. Sci. Technol. Int J.,* vol. 20, issue 2, pp. 679-686, Apr. 2017